MODELING BRINE-ROCK INTERACTIONS IN AN ENHANCED GEOTHERMAL SYSTEM DEEP FRACTURED RESERVOIR AT SOULTZ-SOUS-FORETS (FRANCE): A JOINT APPROACH USING TWO GEOCHEMICAL CODES: FRACHEM AND TOUGHREACT

Laurent André[1], Nicolas Spycher[2], Tianfu Xu[2], François-D. Vuataz[1] and Karsten Pruess[2]*

(1)   Centre of Geothermal Research – c/o Centre of Hydrogeology - Emile Argand 11, CH-2009 Neuchâtel, Switzerland
(2)   Earth Sciences Division - Lawrence Berkeley National Laboratory - Berkeley, CA 94720, USA

December 2006

* Current address: BRGM - Water Division, 3 avenue C. Guillemin, BP 6009, 45060 Orléans Cedex 2, France; l.andre@brgm.fr

EXECUTIVE SUMMARY

The modeling of coupled thermal, hydrological, and chemical (THC) processes in geothermal systems is complicated by reservoir conditions such as high temperatures, elevated pressures and sometimes the high salinity of the formation fluid. Coupled THC models have been developed and applied to the study of enhanced geothermal systems (EGS) to forecast the long-term evolution of reservoir properties and to determine how fluid circulation within a fractured reservoir can modify its rock properties. In this study, two simulators, FRACHEM and TOUGHREACT, specifically developed to investigate EGS, were applied to model the same geothermal reservoir and to forecast reservoir evolution using their respective thermodynamic and kinetic input data. First, we report the specifics of each of these two codes regarding the calculation of activity coefficients, equilibrium constants and mineral reaction rates. Comparisons of simulation results are then made for a Soultz-type geothermal fluid (ionic strength ~1.8 molal), with a recent (unreleased) version of TOUGHREACT using either an extended Debye-Hückel or Pitzer model for calculating activity coefficients, and FRACHEM using the Pitzer model as well.

Despite somewhat different calculation approaches and methodologies, we observe a reasonably good agreement for most of the investigated factors. Differences in the calculation schemes typically produce less difference in model outputs than differences in input thermodynamic and kinetic data, with model results being particularly sensitive to differences in ion-interaction parameters for activity coefficient models. Differences in input thermodynamic equilibrium constants, activity coefficients, and kinetics data yield differences in calculated pH and in predicted mineral precipitation behavior and reservoir-porosity evolution. When numerically cooling a Soultz-type geothermal fluid from 200°C (initially equilibrated with calcite at pH 4.9) to 20°C and suppressing mineral precipitation, pH values calculated with FRACHEM and TOUGHREACT/ Debye-Hückel decrease by up to half a pH unit, whereas pH values calculated with TOUGHREACT/Pitzer increase by a similar amount. As a result of these differences, calcite solubilities computed using the Pitzer formalism (the more accurate approach) are up to about 1.5 orders of magnitude lower. Because of differences in Pitzer ion-interaction parameters, the calcite solubility computed with TOUGHREACT/Pitzer is also typically about 0.5 orders of magnitude lower than that computed with FRACHEM, with the latter expected to be most accurate.

In a second part of this investigation, both models were applied to model the evolution of a Soultz-type geothermal reservoir under high pressure and temperature conditions. By specifying initial conditions reflecting a reservoir fluid saturated with respect to calcite (a reasonable assumption based on field data), we found that THC reservoir simulations with the three models yield similar results, including similar trends and amounts of reservoir porosity decrease over time, thus pointing to the importance of model conceptualization. This study also highlights the critical effect of input thermodynamic data on the results of reactive transport simulations, most particularly for systems involving brines.

INTENTIONALLY LEFT BLANK

TABLE OF CONTENTS

LIST OF FIGURES

LIST OF TABLES

INTENTIONALLY LEFT BLANK

1 INTRODUCTION

This work was initiated through the collaboration between the Centre of Geothermal Research, Neuchâtel, Switzerland (CREGE) and the Earth Sciences Division at Lawrence Berkeley National Laboratory (LBNL), Berkeley, California, USA. During the last several years, these two institutions have been developing reactive transport simulators applicable to the study of coupled thermal, hydrological, and chemical (THC) processes in geothermal systems. The Centre of Hydrogeology of Neuchâtel and then CREGE have been involved since 1998 in the European enhanced geothermal system (EGS) project at Soultz-sous-Forêts, France. The main objective of this project is to build a pilot plant for power production, based on the circulation of a geothermal fluid through a deep fractured reservoir.

The Soultz-sous-Forêts EGS is located in Alsace, about 50 km north of Strasbourg (France). The Soultz area was selected as the European EGS pilot site because of its strong temperature gradient in the sedimentary cover (up to 100°C/km) and its high heat flow, locally reaching 0.15 W/m^2 (Kohl and Rybach, 2001). The geology of the Soultz region is characterized by a graben structure affected by several N-S striking faults. The crystalline basement, covered by 1400 m of Triassic and Tertiary sediments, is composed of three facies in granitic rocks: (1) an unaltered granite in which fracture density is close to zero; (2) a hydrothermally altered granite facies and (3) altered veins within the hydrothermally altered granite (Jacquot, 2000). The hydrothermally altered granite is the most porous facies (Genter et al., 1997) and altered veins are highly fractured. Natural circulation of formation fluid and fluid-rock interaction processes take place mainly within the hydrothermally altered granite, and to a lesser extent within altered veins. Flow in the unaltered granite is essentially nil.

To extract the heat from the Soultz reservoir, three deviated wells have been installed to a depth of 5,000 m, with lower ends separated by 600 m (Figure 1-1). The reservoir encountered at this depth presents an initial temperature of 200°C. One well (GPK3) will be dedicated to the injection of cold water in the granitic reservoir at a rate of about 100 L/s, whereas the two other wells (GPK2 and GPK4), located on both sides of the injector, will be used to produce the formation fluid. At Soultz, the injection–production system has been designed as a closed loop. The fluid used is a formation fluid existing in the altered granite, namely a brine with a total dissolved solids value of around 100,000 ppm. Injection of cooled brine disturbs the equilibrium between the formation fluid and reactive minerals. The resulting change in temperature and pressure in the reservoir, and the forced circulation in fractured granite, will drive geochemical reactions able to affect the physical properties of the reservoir through mineral precipitation and dissolution. The main task of the research on THC coupled modeling for this site has been to forecast the evolution of reservoir porosity and permeability. Different researchers (Durst, 2002, Bächler, 2003, Rabemanana et al. 2003, André et al., 2005) have incrementally built a reactive transport simulator, FRACHEM, able to simulate the main characteristics of the Soultz reservoir at 5 km below the surface, 200°C, 500 bar, and a fluid salinity of around 100,000 ppm.

The reactive transport simulator developed at LBNL, TOUGHREACT (Xu and Pruess, 2001; Xu et al., 2001, 2004a, 2004b, and 2006) was based on introducing reactive chemistry into the code TOUGH2 (Pruess 1991). TOUGHREACT has been applied to different problems, such as CO_2 sequestration in deep saline aquifers and the evolution of water-rock interactions around nuclear

waste disposal sites. A recent upgrade of this code (Zhang et al., 2006a, 2006b) includes the implementation of a Pitzer ion-activity model, allowing model applications involving highly saline brines.

The aim of this study is to investigate the chemical reactions (currently not well known) that take place within the Soultz reservoir at high temperature, elevated pressure, and strong salinity. The main objectives are to determine, as accurately as possible, activity coefficients of dissolved species as well as mineral solubility and dissolution/precipitation rates, to forecast reservoir evolution and porosity variations with time.

Consequently, the first part of this report focuses on comparing values of different computed parameters (activity coefficients, saturation indices, dissolution/precipitation rates), as they are computed by each code according to different methods and/or input thermodynamic data.

The second part of this work relates directly to the enhanced geothermal system of Soultz. Simulations of this reservoir were carried out with FRACHEM to predict the evolution of the reservoir properties. The results obtained with FRACHEM are then compared with the results obtained with TOUGHREACT. Because the TOUGHREACT version used in this report allows selection between an extended Debye-Hückel model and the Pitzer formalism for the calculation of activity coefficients, the two methods have been applied and the predicted respective reservoir evolution then discussed.
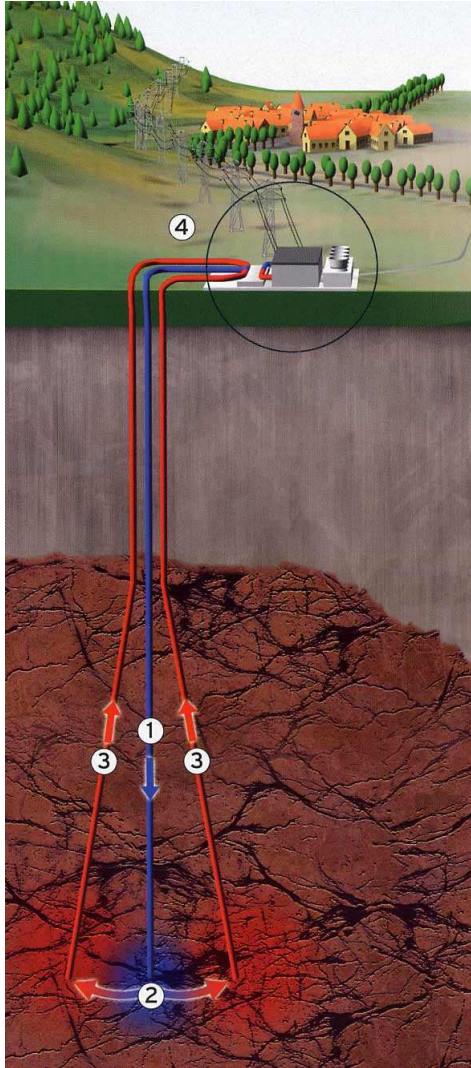
Figure 1-1.   Initial conceptual diagram of the Soultz EGS pilot plant: (1) injection well ; (2) fractured reservoir ; (3) production wells ; (4) power plant.

INTENTIONALLY LEFT BLANK

2   DESCRIPTION OF CODES

This description of the codes is general overview of the computation capabilities of the two simulators. For more details, the reader can consult the TOUGHREACT User's Guide (Xu et al., 2004a) and Xu et al. (2006), as well as the different FRACHEM studies on the Soultz system (Durst, 2002, Bächler et al., 2005).

2.1   FRACHEM

FRACHEM is a THC simulator issued from the combination of two existing codes: FRACTure and CHEMTOUGH2. FRACTure is a 3-D finite-element code for modeling hydrological, transport and elastic processes. It was developed originally for the study of flow-driven interactions in fractured rock (Kohl & Hopkirk, 1995). CHEMTOUGH2 (White, 1995) is a THC code developed after the TOUGH2 simulator (Pruess, 1991), a 3-D numerical model for simulating the coupled transport of water, vapor, noncondensable gas, and heat in porous and fractured media. CHEMTOUGH2 presents the possibility to transport chemical species and to model the chemical water-rock interactions as well as the chemical reactions driven by pressure and temperature changes. The transport and reaction are coupled using a one-step approach.

FRACHEM has been built by introducing geochemical subroutines from CHEMTOUGH2 (White, 1995) into the framework of the code FRACTure (Bächler, 2003; Bächler and Kohl, 2005). After an initialization phase, FRACTure calculates, over each time step, the thermal and hydrological conditions within each element volume and determines the advective flow between each of them. Resulting thermal and hydrological variables are stored in arrays common to FRACTure and the geochemical modules. At this point, the program calculates the chemical reactions using a mass balance/mass action approach, the advective transport of chemical species, and the variations of porosity and permeability. Once this calculation is performed, the porosity and permeability are updated and fed into the FRACTure part of the code. The program then returns to the start of the loop until the end of the simulation time (sequential noniterative approach, SNIA) (Figure 2-1).

FRACHEM has been developed specially for the granitic reservoir of Soultz-sous-Forêts and consequently, specific implementations have been added to the chemical part of this code. The reservoir, at a depth of 5,000 m, contains a brine with about 100,000 ppm total dissolved solids (TDS) and a temperature of 200°C. Considering the high salinity of the geofluid, the Debye-Hückel model, initially implemented in the CHEMTOUGH2 routines to determine the activity coefficients, has been replaced by a Pitzer activity model. It should be mentioned here that the activity coefficients calculations are carried out in an indirect manner by means of another code, TEQUIL (Moller et al., 1998). For a given fluid composition (constant ionic strength), the activity coefficients are determined at different temperatures in the range 50– 200°C using TEQUIL before running FRACHEM. The activity coefficient values obtained at each temperature are regressed as a function of temperature using a polynomial fit, with coefficients then entered into the chemical input file. This approach works well for the case of Soultz simulations because the ionic strength of the circulated fluid remains more or less constant.

Presently, a limited number of minerals are considered, which correspond to the minerals constituting the Soultz granite. The precipitation/dissolution reactions of carbonates (calcite,

dolomite), quartz, amorphous silica, pyrite, and some aluminosilicates (K-feldspar, albite, illite) can be modeled under kinetic constraints. The implemented kinetic-rate laws are specific to each mineral and taken from published experiments conducted at high temperature in NaCl brines. Thermodynamic data (equilibrium constants) are taken mostly from SUPCRT92 (Johnson et al., 1992) and Helgeson et al. (1978) and are functions of temperature and pressure.

Finally, a supplementary module allows the determination of porosity and permeability variations linked with chemical processes occurring in the reservoir. Considering the alteration of the Soultz granite, the flow is assumed to circulate in a medium composed of fractures and grains. Therefore, a combination of fracture model (Norton and Knapp, 1977; Steefel and Lasaga, 1994) and grain model (Bolton et al., 1996) is used to determine the permeability evolution.
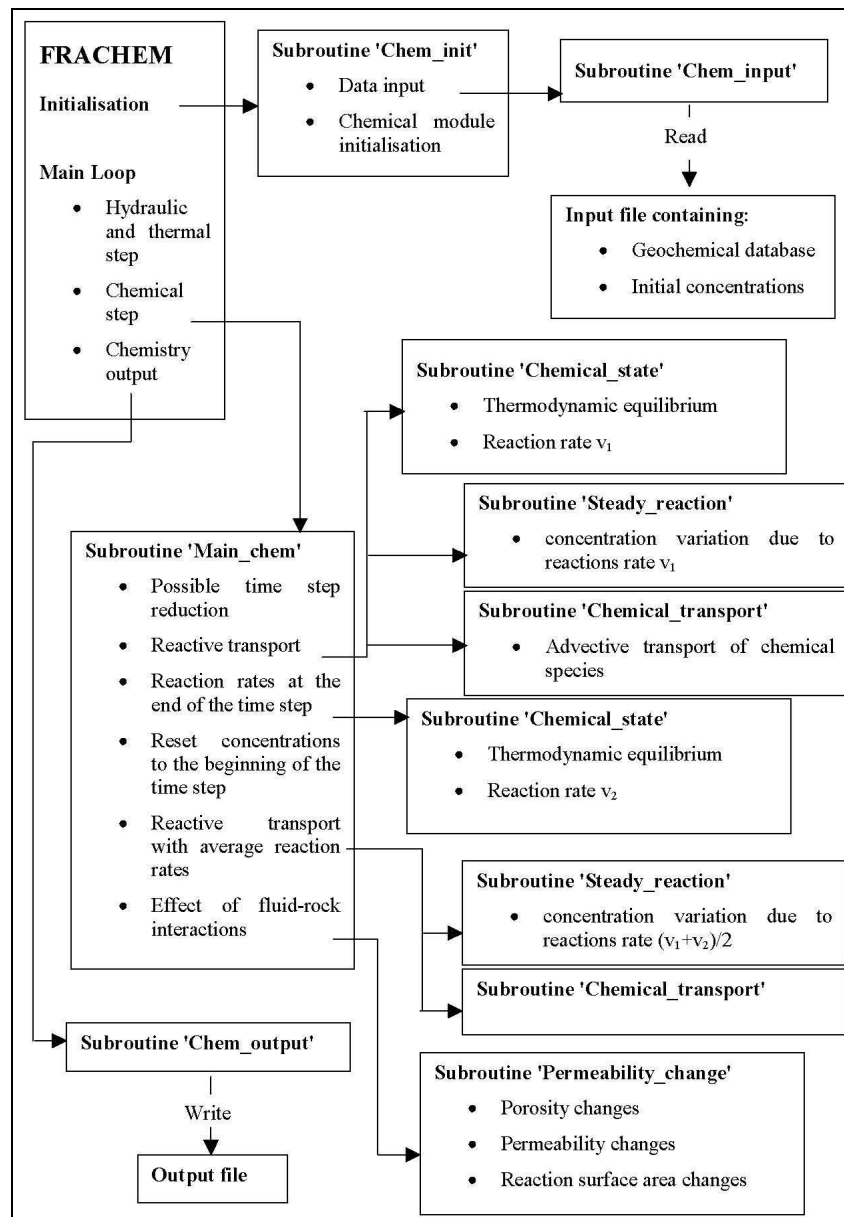
Figure 2-1.   Flow chart of the FRACHEM code (Durst, 2002).

2.2 TOUGHREACT

TOUGHREACT (Xu and Pruess, 2001; Xu et al., 2004a; Xu et al., 2006) was developed by introducing multicomponent reactive transport into the framework of the existing multiphase 3-D finite volume fluid and heat flow code TOUGH2 (Pruess, 1991). It is a THC simulator applicable to a wide range of subsurface conditions and to a variety of reactive fluid and geochemical transport problems. Flow, transport, and chemistry are coupled in a sequential manner (Figure 2-2). Here, a sequential noniterative approach was applied for consistency with the FRACHEM simulations.

TOUGHREACT takes into consideration many processes, such as (1) fluid flow in both liquid and gas phases occurring under pressure, viscous, and gravity forces; (2) heat flow by conduction and convection; (3) diffusion of water vapor and air; (4) thermophysical and geochemical reactions as a function of temperature, such as fluid (gas and liquid) density and viscosity, and thermodynamic and kinetic data for mineral-water-gas reactions; (5) transport of aqueous and gaseous species by advection and molecular diffusion in liquid and gas phases, respectively; (6) temporal changes in porosity, permeability, and unsaturated hydrologic properties owing to mineral dissolution, precipitation and clay swelling. The primary governing equations for multiphase fluid and heat flow, and chemical transport are derived from the principle of mass (or energy) conservation (Pruess, 1987; Pruess et al., 1999). The chemistry computations are based on a mass-balance/mass-action approach (e.g., Reed, 1982). Mass conservation is written in terms of basis species, with distributions governed by the total concentrations of the components.

The code makes use of an input thermodynamic database incorporating equilibrium constants for mass-action equations and parameters for the calculation of activity coefficients. Temperature and pressure ranges are controlled by the applicable range of this thermodynamic database, and the range of the equation of state (EOS) module employed in the multiphase flow computations. For this study, equilibrium constants in the database are given for temperatures ranging from 0 to 300ºC, and pressures of 1 bar up to 100ºC and water saturation pressures above 100ºC. These data come mostly from SUPCRT92 (Johnson et al., 1992). Other thermodynamic and kinetic data are also functions of temperature. The currently released version of the code incorporates an extended Debye-Hückel equation (Helgeson et al., 1981) to compute activity coefficients of charged species and water activity for dilute to moderately saline water (up to ~4 molal for an NaCl-dominant solution). Activity coefficients for dissolved gases such as CO_2(aq) are computed from equations developed by Drummond (1981). Recently, a full Pitzer ion-interaction model was implemented as an option, using the formulation of Harvie et al. (1984) (Zhang et al., 2006a,b; see also Zhang et al., 2004) and ion-interaction parameters re-evaluated and fitted as a function of temperature by Wolery et al. (2004) (as published by Alai et al., 2005). Note that the latter data were modified to incorporate more suitable high-temperature data for $CO_{2(aq)}$ from Rumpf et al. (1994) and Rumpf and Maurer (1993), as discussed later.

Mineral dissolution and precipitation can proceed either subject to local equilibrium or kinetic conditions. For kinetically controlled mineral dissolution and precipitation, a general form of transition-state-theory (TST) rate law is used (Lasaga, 1984; Steefel and Lasaga, 1994; Palandri and Kharaka, 2004). Changes in porosity during the simulation are calculated from changes in mineral volume fractions. Several porosity-permeability and fracture aperture-permeability

relationships are included in the model. Here, fracture porosity is related to permeability using the relationship proposed by Verma and Pruess (1988) and described in Xu et al. (2004a).
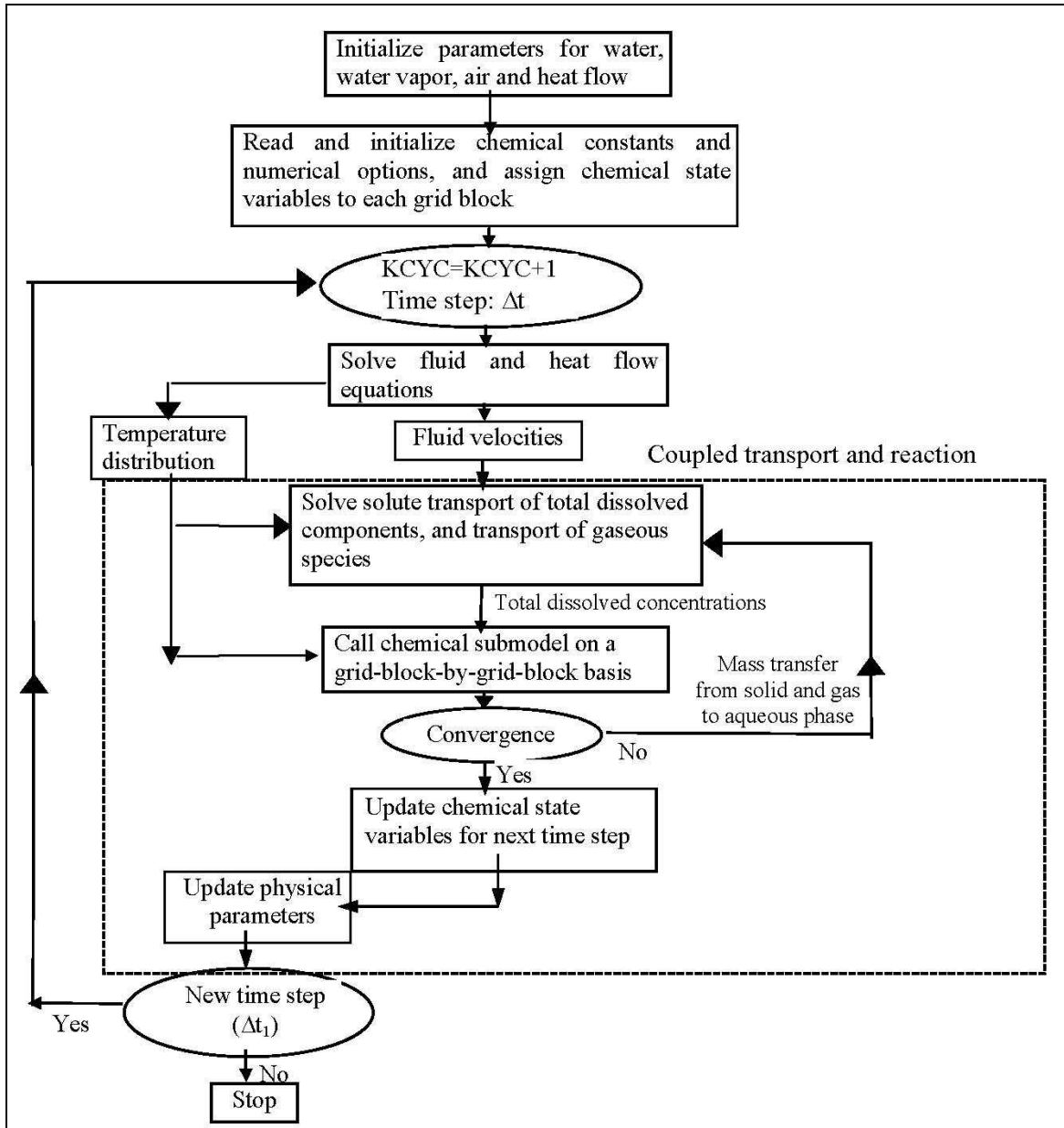
Figure 2-2. Flow chart of the TOUGHREACT simulator (Xu et al., 2004a).

3 CALCULATION OF ACTIVITY COEFFICIENTS

The methods for calculating activity coefficients are described for each code below. An application of these two methods is then presented using a Soultz-type high-salinity geothermal fluid.

3.1 FRACHEM SIMULATIONS

Activity coefficients in FRACHEM simulations are determined in an indirect way using TEQUIL (Moller et al., 1998; http://geotherm.ucsd.edu/tequil/run.html). The latter is used before running FRACHEM to compute aqueous speciation and values of activity coefficients for a given fluid composition and temperature. The activity coefficients for each dissolved species are then entered in a database as regression functions of temperature that are then read by FRACHEM on input.

The TEQUIL application package includes chemical models based on the Pitzer formalism, and calculates liquid-solid-gas equilibria in complex brine systems by globally minimizing the free energy of a system at constant temperature and pressure. Currently, three different models are available in TEQUIL. They are:

- A model of the Na-K-H-Ca-Cl-SO$_4$-HCO$_3$-CO$_3$ -CO$_2$-H$_2$ system for 0 to 250°C (Moller et al., 1998).

- A 25°C model for the Na-K-Ca-Mg-H-Cl-OH-SO$_4$-HCO$_3$-CO$_3$-CO$_2$-H$_2$O system (Harvie et al., 1984).

- A low temperature (-54°C $\leq$ T $\leq$ 25°C) model for the Na-K-Ca-Mg-Cl-SO$_4$-H$_2$O system (Spencer et al., 1990).

In this study, we applied the first model listed above. Using this model, total concentrations obtained from chemical analyses (Table 3-1) were input into TEQUIL, which then computed speciation (Table 3-1) and corresponding activity coefficients. Computations were done using a typical Soultz fluid at a temperature of 200°C. This fluid was initially equilibrated with calcite and anhydrite at 200°C, which resulted in a decrease of Ca^{+2} and SO$_4$$^{-2}$ concentrations (compared to input concentrations) due to precipitation of calcite and anhydrite. The pH value of 4.9 at 200°C was calculated from the equilibration with calcite and input total aqueous carbonate concentration. Using the fluid composition at 200°C, TEQUIL was then used to numerically cool the solution, recompute pH, and determine activity coefficients at temperatures down to 20°C. It should be noted that the cooling simulation was performed without allowing reactions with gases or minerals.

Mg, Fe, and Al are not included in the TEQUIL database. For this reason, the geochemical program EQ3nr (Wolery, 1992) was applied to determine the activity coefficients of Mg^{2+}, Fe^{2+} and Al^{3+} by using the Pitzer model and the EQ3nr thermodynamic database *data0.hmw* (Harvie et al. 1984).

Activity coefficients determined in this way were then input into FRACHEM as polynomial functions of temperature, for the specific ionic strength of the fluid (nearly constant in our case).

Activity coefficients were then compared with activity coefficients computed with TOUGHREACT as discussed below (Table 3-2).

Activity coefficients by themselves do not provide a means to evaluate differences in chemical behavior predicted by the various codes. Activity coefficients need to be considered together with results of speciation calculations, as expressed by the computed activities of dissolved species (i.e., the product of individual molalities and activity coefficients). This is because ion association and complexation may be implicitly accounted for by activity coefficients (e.g., as done typically with Pitzer models), or explicitly computed with the use of secondary species (e.g., as done with Debye-Hückel models). Therefore, two codes could compute quite different activity coefficients for a given primary aqueous species, but quite similar activities (and thus similar chemical behavior). For this reason, activities of aqueous species computed with FRACHEM are also presented (Table 3-3), for direct comparison with the results of TOUGHREACT.

Table 3-1. Fluid composition from field data (circulation test of 03/12/1999) and modeled composition of the same fluid after equilibration with calcite and anhydrite at 200°C using TEQUIL (Na-K-H-Ca-Cl-SO_4-HCO_3-CO_3-CO_2-SiO_2-H_2O system).

Analyte	Total concentrations (molal)	Species	Concentrations of individual species computed by TEQUIL (molal)
		pH	4.9 (at 200°C)
Σ Na	1.148	Na^+	1.148
Σ K	73.40×10^{-3}	K^+	$73.4 \ 10^{-3}$
Σ Ca	$0.1695 / 0.1193^{**}$	Ca^{++}	0.1190
Σ Cl	1.648	Cl^-	1.64800
Σ $S^{(VI)}$	$1.771 \times 10^{-3} / 0.9817 \times 10^{-3\ **}$	SO_4^{--}	$0.711 \ 10^{-3}$
Σ Si	6.060×10^{-3}	H_4SiO_4	$6.060 \ 10^{-3}$
Σ C	$4.250 \times 10^{-2} / 4.277 \times 10^{-2\ **}$	OH^-	$1.908 \ 10^{-6}$
Σ Mg	3.210×10^{-3}	HCO_3^-	$1.539 \ 10^{-3}$
Σ Fe	2.614×10^{-3}	CO_3^{--}	$2.038 \ 10^{-7}$
Σ Al	3.700×10^{-5}	$CaCO_{3(aq)}$	$7.026 \ 10^{-7}$
		$CO_{2(aq)}$	$4.123 \ 10^{-2}$
		$CaHCO_3^+$	$1.111 \ 10^{-18}$
		$CaSO_{4(aq)}$	$2.707 \ 10^{-4}$

** After equilibration with calcite and anhydrite

3.2 TOUGHREACT SIMULATIONS

In TOUGHREACT, activity coefficients are computed in the code as a function of the current (true) ionic strength. In the version used for his study (V3.2ymp), the user has the choice of an extended Debye-Hückel model (Helgeson et al., 1981) for solution of moderate ionic strengths, or a Pitzer model following Harvie et al. (1984) for more saline solutions (Zhang et al., 2006a,b; see also Zhang et al., 2004). Here, we compare the results of these two models with the FRACHEM/TEQUIL results discussed earlier.

3.2.1 TOUGHREACT with Extended Debye-Hückel model (Tr-DH)

The Debye-Hückel model with TOUGHREACT was selected by setting the input flag MOPR(9) equal to 0. The computation was carried out with the *ThermXu4.dat* database, which consists

essentially of thermodynamic data from the SUPCRT92 package (Johnson et al., 1992) (see also Section 5). For consistency with the TEQUIL simulation, a TOUGHREACT speciation calculation was first run at 200°C using the fluid composition in Table 3-1 and fixing the pH at a value of 4.9, as determined earlier from the TEQUIL simulation. As previously, the resulting fluid was then numerically cooled without allowing reaction with minerals, yielding activity coefficients and activities at different temperatures down to 20°C (Tables 3-2 and 3-3).

3.2.2 TOUGHREACT with Pitzer model (Tr-Pitzer)

The Pitzer model with TOUGHREACT was selected by setting the input flag MOPR(9) equal to 2. As previously, the computation was carried out using the database *ThemXu4.dat* for equilibrium constants of minerals and secondary species. The EQ3/6 *data0.ypf* database (Wolery et al., 2004, as published by Alai et al., 2005) is used for all Pitzer ion-interaction parameters, except for the $CO_{2(aq)}$ parameters, which had to be revised for this study. Earlier simulations using the original *data0.ypf* database (André et al., 2006) showed that this database could not reasonably reproduce the solubility of calcite at temperatures above about 100°C. This discrepancy was eventually traced to the Pitzer ion-interaction parameters for $CO_{2(aq)}$ in the database. These parameters (after He and Morse, 1993) were found to yield erroneous activity coefficients for $CO_{2(aq)}$ when extrapolated at temperatures above about 100°C, in large part because these authors fitted their data (up to 90°C) to a polynomial as a function of temperature, using the same number of data points as the number of fit coefficients. For this reason, we replaced the $CO_{2(aq)}$ data in the *data0.ypf* database with values refitted from ion-interaction parameters reported by Rumpf et al. (1994) and Rumpf and Maurer (1993) for temperatures up to 160°C, which extrapolate smoothly and with reasonable accuracy up to 200°C. The *data0.ypf* database revised with these data was used for all Tr-Pitzer simulations presented in this report.

Secondary species used in the calculations were selected specifically to be consistent with the secondary species in use with the *data0.ypf* Pitzer database. The input flags MOPR(10) and MOPR(11) were set to 3 and 1, respectively, for a fluid ionic strength less than 5 (Zhang et al., 2006a). TOUGHREACT was then run with the same fluid composition as previously (Table 3-1), starting with a pH of 4.9 at 200°C and cooling the solution down to 20°C without allowing mineral reaction. The computed activity coefficients and activities were then compared with the data from the other models (Tables 3-2 and 3-3).

Table 3-2. Computed activity coefficients (molal scale) as a function of temperature, using the fluid composition given in Table 3-1.

Species	Model	20°C	50°C	80°C	110°C	140°C	170°C	200°C
Al^{+++}	FRACHEM[1]	0.3540	0.2400	0.1310	0.0590	0.0209	0.0006	0.0001
	Tr-DH	0.0315	0.0159	0.0073	0.0032	0.0014	0.0006	0.0003
	Tr-Pitzer	0.0007	0.0003	0.0001	0.0001	0.0000	0.0000	0.0000
AlO_2^-	FRACHEM [2]	/	/	/	/	/	/	/
	Tr-DH	0.675	0.685	0.662	0.623	0.577	0.528	0.475
	Tr-Pitzer	0.570	0.534	0.485	0.441	0.403	0.370	0.341
Ca^{++}	FRACHEM	0.296	0.285	0.257	0.222	0.182	0.142	0.104
	Tr-DH	0.191	0.149	0.108	0.077	0.054	0.037	0.025
	Tr-Pitzer	0.041	0.100	0.178	0.256	0.301	0.289	0.224
$CaCO_{3(aq)}$	FRACHEM	1.000	1.000	1.000	1.000	1.000	1.000	1.000
	Tr-DH	1.000	1.000	1.000	1.000	1.000	1.000	1.000
	Tr-Pitzer	1.000	1.000	1.000	1.000	1.000	1.000	1.000
$CaHCO_3^+$	FRACHEM	0.490	0.488	0.471	0.444	0.411	0.372	0.329
	Tr-DH	0.613	0.642	0.640	0.620	0.591	0.555	0.512
	Tr-Pitzer	0.445	0.405	0.368	0.336	0.305	0.272	0.237
$CaSO_{4(aq)}$	FRACHEM	1.000	1.000	1.000	1.000	1.000	1.000	1.000
	Tr-DH	1.000	1.000	1.000	1.000	1.000	1.000	1.000
	Tr-Pitzer	1.000	1.000	1.000	1.000	1.000	1.000	1.000
Cl^-	FRACHEM	0.585	0.559	0.528	0.492	0.453	0.409	0.363
	Tr-DH	0.675	0.685	0.662	0.623	0.577	0.528	0.475
	Tr-Pitzer	0.613	0.644	0.646	0.630	0.599	0.554	0.494
$CO_{2(aq)}$	FRACHEM	1.371	1.356	1.344	1.334	1.325	1.318	1.311
	Tr-DH	1.420	1.363	1.336	1.332	1.343	1.365	1.394
	Tr-Pitzer	1.418	1.346	1.316	1.310	1.318	1.335	1.355
CO_3^{--}	FRACHEM	0.038	0.030	0.022	0.016	0.010	0.006	0.004
	Tr-DH	0.203	0.157	0.114	0.080	0.056	0.039	0.026
	Tr-Pitzer	0.095	0.070	0.044	0.024	0.011	0.004	0.001
Fe^{++}	FRACHEM[1]	0.347	0.294	0.224	0.154	0.093	0.049	0.022
	Tr-DH	0.210	0.157	0.110	0.076	0.051	0.035	0.023
	Tr-Pitzer	0.039	0.027	0.018	0.013	0.009	0.006	0.003
H^+	FRACHEM	1.084	1.051	0.997	0.934	0.865	0.792	0.716
	Tr-DH	0.575	0.621	0.638	0.637	0.623	0.600	0.568
	Tr-Pitzer	0.990	0.874	0.779	0.696	0.615	0.529	0.438
HCO_3^-	FRACHEM	0.389	0.374	0.347	0.310	0.267	0.222	0.178
	Tr-DH	0.637	0.660	0.651	0.624	0.588	0.547	0.501
	Tr-Pitzer	0.613	0.592	0.531	0.446	0.350	0.255	0.172
K^+	FRACHEM	0.653	0.689	0.689	0.667	0.630	0.581	0.523
	Tr-DH	0.616	0.644	0.641	0.620	0.589	0.552	0.509
	Tr-Pitzer	0.603	0.589	0.563	0.531	0.495	0.452	0.402

Species	Model	20°C	50°C	80°C	110°C	140°C	170°C	200°C
Mg^{++}	FRACHEM [1]	0.371	0.296	0.221	0.154	0.100	0.060	0.032
	Tr-DH	0.218	0.161	0.112	0.076	0.051	0.034	0.022
	Tr-Pitzer	0.417	0.301	0.224	0.175	0.140	0.110	0.080
Na^+	FRACHEM	0.741	0.784	0.783	0.754	0.706	0.645	0.574
	Tr-DH	0.654	0.669	0.651	0.616	0.574	0.528	0.478
	Tr-Pitzer	0.691	0.675	0.639	0.597	0.548	0.494	0.433
OH^-	FRACHEM	0.431	0.411	0.380	0.340	0.293	0.244	0.197
	Tr-DH	0.774	0.753	0.698	0.631	0.564	0.498	0.434
	Tr-Pitzer	0.633	0.600	0.557	0.513	0.468	0.420	0.369
$SiO_{2(aq)}$	FRACHEM	1.315	1.272	1.236	1.208	1.183	1.163	1.145
	Tr-DH	1.000	1.000	1.000	1.000	1.000	1.000	1.000
	Tr-Pitzer	1.333	1.332	1.313	1.277	1.226	1.163	1.091
SO_4^{--}	FRACHEM	0.048	0.043	0.034	0.025	0.017	0.010	0.006
	Tr-DH	0.183	0.148	0.111	0.082	0.059	0.042	0.030
	Tr-Pitzer	0.092	0.079	0.060	0.044	0.031	0.021	0.013

[1] Activity coefficients calculated with EQ3nr (Wolery 1992) using with the Pitzer model – this species is not included in the Tequil database.
[2] In FRACHEM, aluminium is only considered under the form Al^{+3}.

Table 3-3. Computed activities (in log molal except for H_2O) as a function of temperature, using the fluid composition given in Table 3-1.

Species	Model	20°C	50°C	80°C	110°C	140°C	170°C	200°C
H_2O	**FRACHEM**	0.952	0.952	0.952	0.953	0.954	0.955	0.957
	Tr-DH	0.950	0.952	0.954	0.956	0.959	0.962	0.966
	Tr-Pitzer	0.949	0.949	0.948	0.949	0.950	0.951	0.953
Al^{+++}	**FRACHEM** [1]	-4.88	-5.05	-5.31	-5.66	-6.11	-6.67	-7.36
	Tr-DH	-5.94	-6.27	-6.76	-8.02	-9.94	-11.84	-13.71
	Tr-Pitzer	-7.60	-7.96	-8.35	-9.00	-10.20	-11.58	-13.04
AlO_2^-	**Frachem** [2]	/	/	/	/	/	/	/
	Tr-DH	-12.65	-9.97	-7.69	-6.50	-6.08	-5.78	-5.57
	Tr-Pitzer	-9.74	-7.74	-6.09	-5.08	-4.86	-4.87	-4.90
Ca^{++}	**FRACHEM**	-1.45	-1.47	-1.51	-1.58	-1.66	-1.77	-1.91
	Tr-DH	-1.69	-1.79	-1.93	-2.08	-2.24	-2.41	-2.60
	Tr-Pitzer	-2.31	-1.93	-1.68	-1.53	-1.47	-1.49	-1.60
$CaCO_{3(aq)}$	**FRACHEM**	-5.99	-6.04	-6.06	-6.08	-6.10	-6.13	-6.15
	Tr-DH	-8.04	-7.53	-7.15	-6.90	-6.67	-6.46	-6.28
	Tr-Pitzer	-6.45	-5.79	-5.39	-5.24	-5.24	-5.29	-5.37
$CaHCO_3^+$	**FRACHEM**	-18.26	-18.27	-18.28	-18.31	-18.34	-18.38	-18.44
	Tr-DH	-4.08	-4.02	-3.96	-3.92	-3.87	-3.81	-3.75
	Tr-Pitzer	-3.64	-3.26	-3.00	-2.86	-2.81	-2.81	-2.84
$CaSO_{4(aq)}$	**FRACHEM**	-4.24	-3.89	-3.70	-3.61	-3.60	-3.62	-3.57
	Tr-DH	-3.79	-3.84	-3.89	-3.93	-3.96	-3.98	-3.99
	Tr-Pitzer	-4.29	-3.89	-3.64	-3.48	-3.40	-3.35	-3.34
Cl^-	**FRACHEM**	-0.07	-0.09	-0.11	-0.15	-0.18	-0.23	-0.28
	Tr-DH	0.01	0.01	-0.02	-0.05	-0.10	-0.15	-0.21
	Tr-Pitzer	0.00	0.03	0.03	0.02	-0.01	-0.04	-0.09
$CO_{2(aq)}$	**FRACHEM**	-1.25	-1.25	-1.26	-1.26	-1.26	-1.27	-1.27
	Tr-DH	-1.23	-1.25	-1.26	-1.26	-1.25	-1.24	-1.24
	Tr-Pitzer	-1.30	-1.32	-1.33	-1.34	-1.33	-1.33	-1.32
CO_3^{--}	**FRACHEM**	-9.17	-9.09	-9.05	-9.04	-9.07	-9.11	-9.15
	Tr-DH	-9.62	-9.31	-9.13	-9.07	-9.03	-9.04	-9.11
	Tr-Pitzer	-7.41	-7.43	-7.61	-7.95	-8.37	-8.80	-9.20
Fe^{++}	**FRACHEM** [1]	-3.05	-3.11	-3.23	-3.40	-3.62	-3.89	-4.24
	Tr-DH	-3.36	-3.48	-3.64	-3.84	-4.11	-4.52	-5.10
	Tr-Pitzer	-3.99	-4.15	-4.32	-4.48	-4.64	-4.84	-5.08
H^+	**FRACHEM**	-4.44	-4.34	-4.34	-4.41	-4.54	-4.70	-4.90
	Tr-DH	-4.19	-4.20	-4.28	-4.37	-4.52	-4.70	-4.90
	Tr-Pitzer	-5.33	-5.18	-5.07	-4.97	-4.90	-4.86	-4.90
HCO_3^-	**FRACHEM**	-3.22	-3.23	-3.27	-3.32	-3.38	-3.47	-3.56
	Tr-DH	-3.44	-3.34	-3.31	-3.34	-3.39	-3.46	-3.55
	Tr-Pitzer	-2.37	-2.44	-2.59	-2.83	-3.10	-3.38	-3.64

Species	Model	20°C	50°C	80°C	110°C	140°C	170°C	200°C
K^+	FRACHEM	-1.32	-1.30	-1.30	-1.31	-1.34	-1.37	-1.42
	Tr-DH	-1.35	-1.34	-1.35	-1.38	-1.41	-1.45	-1.50
	Tr-Pitzer	-1.35	-1.36	-1.38	-1.41	-1.44	-1.48	-1.53
Mg^{++}	FRACHEM [1]	-2.92	-3.02	-3.15	-3.31	-3.49	-3.72	-3.99
	Tr-DH	-3.26	-3.37	-3.53	-3.70	-3.88	-4.08	-4.30
	Tr-Pitzer	-2.87	-3.02	-3.14	-3.25	-3.35	-3.45	-3.59
Na^+	FRACHEM	-0.07	-0.05	-0.05	-0.06	-0.09	-0.13	-0.18
	Tr-DH	-0.17	-0.17	-0.20	-0.23	-0.28	-0.33	-0.40
	Tr-Pitzer	-0.10	-0.11	-0.14	-0.17	-0.20	-0.25	-0.30
OH^-	FRACHEM	-9.74	-8.96	-8.29	-7.72	-7.23	-6.80	-6.43
	Tr-DH	-9.99	-9.10	-8.35	-7.75	-7.23	-6.78	-6.40
	Tr-Pitzer	-8.85	-8.12	-7.56	-7.16	-6.86	-6.62	-6.41
$SiO_{2(aq)}$	FRACHEM	-2.10	-2.11	-2.13	-2.14	-2.15	-2.15	-2.16
	Tr-DH	-2.22	-2.22	-2.22	-2.22	-2.22	-2.22	-2.22
	Tr-Pitzer	-2.09	-2.09	-2.10	-2.11	-2.13	-2.15	-2.18
SO_4^{--}	FRACHEM	-4.36	-4.44	-4.58	-4.74	-4.91	-5.13	-5.39
	Tr-DH	-4.18	-4.26	-4.35	-4.44	-4.54	-4.66	-4.81
	Tr-Pitzer	-4.07	-4.17	-4.35	-4.54	-4.75	-4.95	-5.17

[1] Activity coefficients calculated with EQ3nr (Wolery 1992) using with the Pitzer model – this species is not included in the Tequil database.

[2] In FRACHEM, aluminium is only considered under the form Al^{+3}.

3.3 DISCUSSION

The activity coefficients and the activities of dissolved species computed with the three models (FRACHEM, Tr-DH and Tr-Pitzer) are compared in Tables 3-2 and 3-3, and also plotted in Figures 3-1 and 3-2. The agreement is reasonably good for Na^+, K^+ and SiO_2; however, important divergences occur with Ca^{2+} and Mg^{2+}, primarily between simulations making use of the Pitzer formalism (FRACHEM and Tr-Pitzer) and the extended Debye-Hückel model (Tr-DH). As mentioned earlier, activities (and not activity coefficients) drive the chemical reactions. Therefore, comparing activities rather than activity coefficients is generally more instructive. However, differences in computed activities for a given species may not necessarily indicate differences in simulated chemical behavior, if the species is not a dominant one. For example, in our case, computed activities of Al^{+++} are quite different (Table 3-3) but the dominant species in the simulation is AlO_2^-, for which computed activities do not differ significantly between models (thus not significantly affecting simulation results).

Starting at pH 4.9 at 200°C, all three models predict an initial pH decrease with decreasing temperature (see the log activity of H+ in Table 3-3). However, pH values predicted with Tr-Pitzer start to increase as the temperature decreases below 150°C, and reach about 5.3 at 20°C. In contrast, pH values predicted with FRACHEM decrease to a minimum of around 4.3 at 80°C, then slightly increase to end up around 4.4 at 20°C. With the Tr-DH model, no trend reversal is observed, and the pH keeps decreasing with temperature to about 4.2 at 20°C (Table 3-3). Note that during the circulation test occurring in 1997 in Soultz, a pH of 4.8 was measured on line, after the heat exchanger outlet, at a temperature of 60–65°C (Durst, 2002). This value is within

the range of the calculated pH values, but not much below the initial pH of 4.9 at 200°C. In the real system, precipitation of aluminum silicates by cooling could take place, which would then have a tendency to drive pH up. Therefore, these simple cooling simulations are likely to underestimate pH. It should be kept in mind that mineral precipitation during cooling was intentionally suppressed, here, such that model comparisons with respect to activity coefficients could be made for identical fluid compositions. More realistic simulations of field conditions are discussed in Section 5.

At the same initial pH of 4.9 at 200°C, the range of calcite saturation indices predicted by the three models spans about 0.9 log(Q/K) units (Table 3-4), representing the difference between the Tr-Pitzer and Tr-DH models. This difference is primarily attributed to the activity coefficient of Ca^{++} (Table 3-2). The larger Ca^{++} activity coefficient (by up to one order of magnitude) computed using the Pitzer formalism, compared to the extended Debye-Hückel equation, translate to about the same range in Ca^{++} activity increase (Table 3-3), and thus to a solubility decrease of close to 1 log(Q/K) unit at 200°C. The difference in calcite saturation index computed by TR-Pitzer and FRACHEM is only about 0.3 log(Q/K) units at 200°C. These differences at 200°C increase at lower temperatures (Table 3-3), as a result of the pH differences discussed above, which are themselves also the result of activity coefficient effects. For all three models, however, a similar trend of decreasing calcite log(Q/K) values (increasing solubility) with decreasing temperature is observed (Table 3-4, see also Figure 3-3). This is consistent with literature data (e.g., Ellis, 1963; Newton and Manning, 2002) indicating retrograde calcite solubility in pure water and NaCl solutions.

The fluid saturation with respect to quartz was also investigated (Table 3-4). Results show minor differences in the quartz solubilities computed by Tr-Pitzer and Tr-DH at all temperatures, even though Tr-DH assumes a unit activity coefficient for $SiO_{2(aq)}$. These two models, however, predict significantly lower solubility than FRACHEM at low temperature, the result of differences in input solubility data (Section 5). Note that quartz precipitation at temperatures below about 150°C becomes increasingly kinetically retarded, such that the variability of solubility data at low temperature has not much bearing on the results of THC simulations such as those presented later in Section 6.

Table 3-4. Saturation Index of quartz and calcite minerals computed as a function of temperature, using the fluid composition given in Table 3-1.

		Log (Q/K)					
		50°C	80°C	110°C	140°C	170°C	200°C
Calcite	Tr-DH	-2.41	-2.00	-1.68	-1.34	-1.000	-0.672
	Tr-Pitzer	-0.670	-0.250	-0.020	0.093	0.165	0.237
	FRACHEM	-1.66	-1.32	-0.960	-0.611	-0.287	0.000
Quartz	Tr-DH	1.23	0.937	0.689	0.483	0.311	0.166
	Tr-Pitzer	1.36	1.056	0.796	0.572	0.377	0.204
	FRACHEM	0.355	0.166	0.008	-0.125	-0.241	-0.343

Figure 3-1. Evolution of logarithm of activities with temperature for selected dissolved species: Ca^{++}, HCO_3^-, H^+ and CO_3^{--}. For each species, activities have been computed with FRACHEM (black continuous lines), Tr-DH (black dashed lines) and Tr-Pitzer (grey dashed lines).
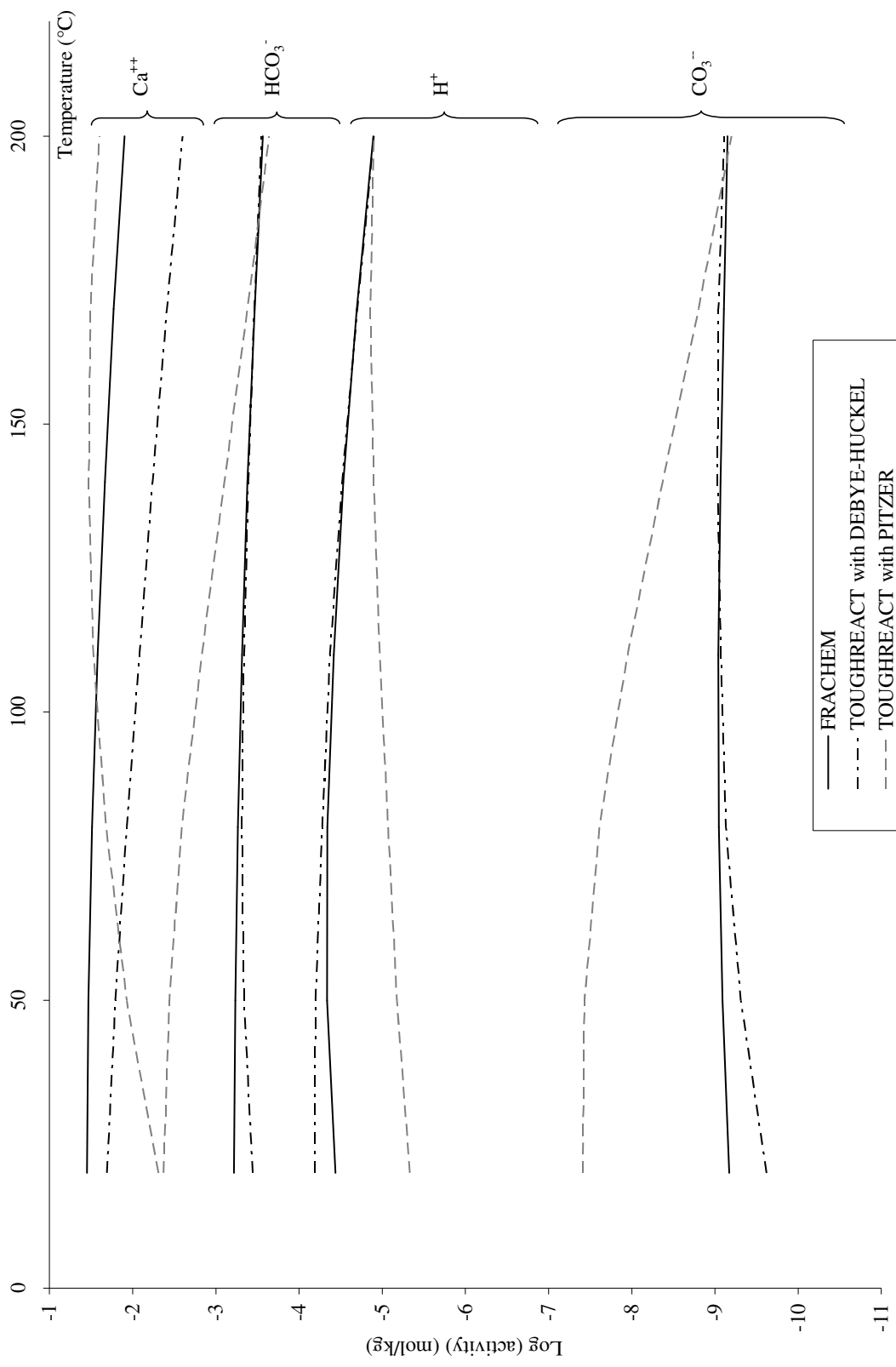
Figure 3-2. Evolution of logarithm of activities with temperature for selected dissolved species: Na+, K+, SiO2, Mg++ and SO4--. For each species, activities have been computed with FRACHEM (black continuous lines), Tr-DH (black dashed lines) and Tr-Pitzer (grey dashed lines).
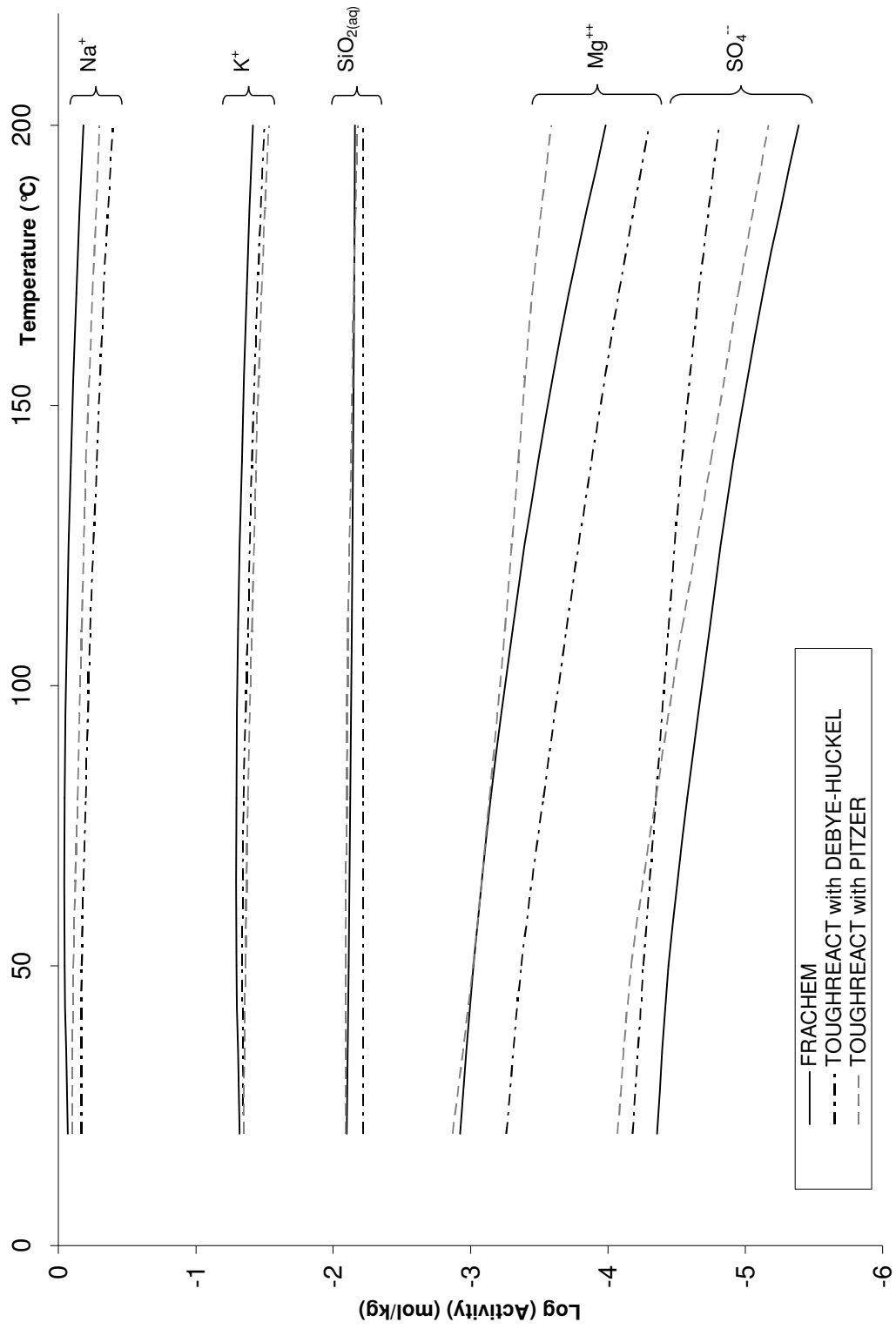
To further investigate the predicted trends of pH and calcite saturation with temperature, the same simple cooling simulation (without mass transfer to minerals or gases) was repeated with several other popular geochemical codes, with thermodynamic databases and activity coefficient models as follows:

- PHREEQC 2.12 (Parkhurst and Appelo, 1999) with the following databases (as released with version 2.12): *phreeqc*.dat *431 2005-08-23* with the Davies equation; *llnl.dat 85 2005-02-0* with the extended Debye-Hückel equation; and the Pitzer model implemented with database *pitzer.dat 2005-11-16*.

- EQ3/6 8.0 (Wolery and Jareck, 2003) with (1) the "b-dot" extended Debye-Hückel model of Helgeson (1969) and database *data0.ymp*; (2) the Pitzer model and database *data0.hmw* (after Harvie et al., 1984); and (3) the Pitzer model and the same revised *data0.ypf* database as used with Tr-Pitzer (Wolery et al., 2004, as published in Alai et al. (2005) except for revisions to $CO_{2(aq)}$ ion interaction parameter after Rumpf et al. 1994 and Rumpf and Maurer 1993).

- SOLVEQ/CHILLER (Reed, 1998; Reed and Spycher, 1998), which incorporates the extended Debye-Hückel model of Helgeson et al. (1981) and the same equilibrium constants as used with Tr-DH (SUPCRT92, Johnson et al., 1992).

These codes were applied to the same fluid composition as used with the three other models (FRACHEM, Tr-DH and Tr-Pitzer) (Table 3-1) with an input brine pH of 4.9 at 200ºC. However, in this case, the minor components Al, Fe, and Mg were excluded from the system, such that TEQUIL could be used directly (in place of FRACHEM). Note that the calcite equilibrium constant is nearly the same in all the databases considered (Section 5). It was also verified that only those secondary aqueous species called for by the different activity coefficient models were included in simulations.

The most remarkable parameters, pH and calcite saturation index (Figure 3-3) show significant variations. Using the Pitzer formalism, some divergences appear with the use of different ion-interaction parameters. The results of EQ3/6 with the revised *data0.ypf* Pitzer database closely match the TR-Pitzer results, as expected because both models make use of the same database. Therefore, the trend of mostly increasing pH with decreasing temperature computed with Tr-Pitzer is confirmed by the EQ3/6 results. Both models also predict lower calcite solubilities than TEQUIL (typically by about 0.5 log(Q/K) units) (Figure 3-3). Nevertheless, all models yield a consistent trend of calcite retrograde solubility. Because of similarities between databases, EQ3/6 with the Harvie et al. (1984) Pitzer database yield results fairly close to those of TEQUIL. EQ3/6 with the "b-dot" model also matches surprisingly well the results of TEQUIL. The same extended Debye-Hückel equation and parameters are implemented in Tr-DH and SOLVEQ/CHILLER, and therefore the results of both these models match closely. Note that the results from the PHREEQC-Pitzer model are more in line with the Debye-Hückel models, whereas the standard PHREEQC model (Davies equation) matches somewhat more closely the TR-Pitzer results (Figure 3-3). Although this may seem counterintuitive, these differences result from the fact that the Davies equation typically predicts a sharper rise in activity coefficient values at elevated ionic strength compared to the other extended Debye-Hückel models (e.g., Langmuir 1997). Also, the Pitzer ion-interaction parameters in the PHREEQC Pitzer database are temperature-independent and therefore not really applicable here.

These results illustrate the importance of activity coefficients when dealing with concentrated solutions. The variation of activity coefficients with temperature is critical and often the weak point of Pitzer databases available from the literature. For example, in some databases, ion-interaction parameters may be set to 0 or fixed values for different temperatures. Avoiding "double counting" between interaction parameters and secondary species is also critical. Even with the simpler Debye-Hückel model, it is important to keep consistency between the data used to compute activity coefficients and the types of secondary aqueous species and their dissociation constants. For application to Soultz-type concentrated fluids at elevated temperatures, a Pitzer approach is definitely favored, with preference given to the TEQUIL database because it was developed specifically for geothermal applications at moderate ionic strengths. The relatively recent EQ3/6 database *data0.ypf*, as revised in this study, is expected to be most accurate for applications below 150°C and very high ionic strengths. As shown later, for reactive transport simulations of the Soultz system, differences in computed calcite solubility using these different databases can be partly offset by specifying initial conditions of fluid saturation with respect to calcite in the reservoir. This is accomplished by adjusting pH, bicarbonate, and/or calcium concentrations, whichever has highest uncertainty, to reflect initial saturation of the fluid with respect to calcite. In this respect, the conceptual model is just as important as the thermodynamic data input into the numerical model.
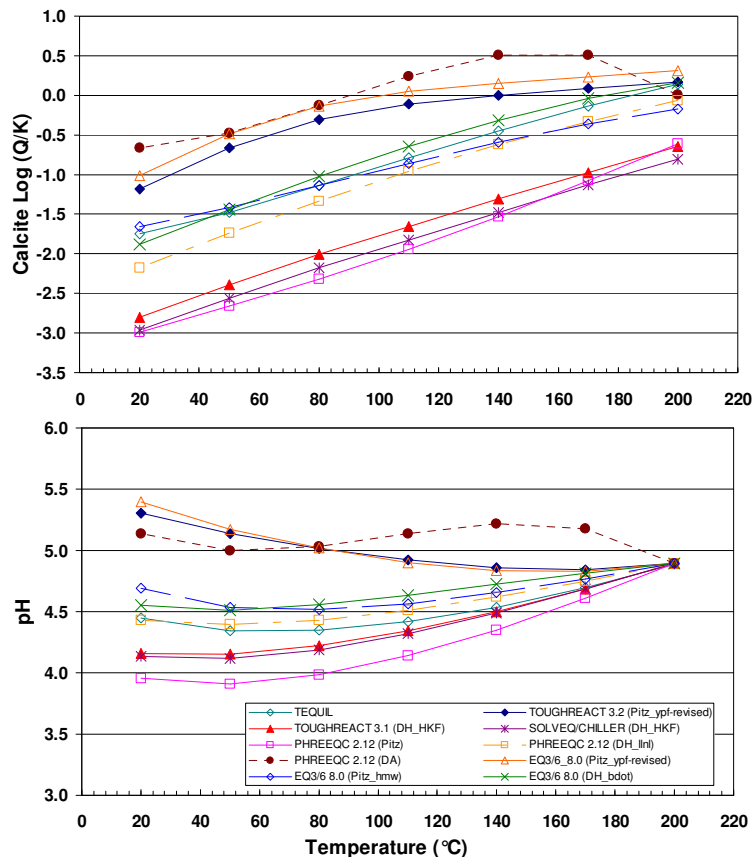

Figure 3-3. Cooling simulation of a Soultz-type fluid (Table 3-1): calcite saturation index and pH predicted as a function of temperature, using various codes and thermodynamic databases (see text). To keep the fluid composition identical in all cases (except for H+, which is set by specifying a pH of 4.9 at 200°C), no minerals are allowed to form during cooling.

4 THE KINETIC RATE LAWS

4.1 FRACHEM

A general kinetic model has been adopted to explain the dissolution/precipitation reactions of minerals. Its overall form is the transition state theory (TST)-derived equation (e.g., Lasaga et al., 1994) expressed as

$$v = k_m s_m \left(1 - \left(\frac{Q_m}{K_m}\right)^\mu\right)^n \qquad \text{Eq. 1}$$

where v is the reaction rate (mol s^{-1} kg$_{water}$$^{-1}$), k_m is the rate constant (mol s^{-1} m^{-2}), s_m is the surface area of mineral in contact with fluid (m^2 kg$_{water}$$^{-1}$), μ and η are positive empirical parameters, and Q_m and K_m are the ion activity product and equilibrium constant for the mineral reaction, respectively. Positive values of v correspond to dissolution rates, whereas negative values refer to precipitation rates. In FRACHEM, rate laws more or less following Equation 1 were specifically coded for each mineral, using published parameters (k_m, μ and η) determined from experimental data obtained at high temperature in NaCl brines (Table 4-1).

Table 4-1. Mineral dissolution and precipitation rates used in FRACHEM

Reaction rates laws		sources
Calcite dissolution rate $r_d = \left(1.643\text{x}10^{-1}\, a_{H^+} + 1.11\text{x}10^{-5}\right) \dfrac{T}{321.15}$ $\left[\exp\left(\dfrac{(T - 321.15)\left(-151.94\ln(a_{H^+}) + 545.91\right)}{321.15\,T}\right)\right] s\left(1 - \dfrac{Q}{K}\right)$	Eq. 2	Sjöberg & Rickard (1984)
Calcite precipitation rate $r_p = 1.927\text{x}10^{-2}\, T \exp\left(\dfrac{-41840}{RT}\right) s \left(\dfrac{Q}{K} - 1\right)^{1.93} \quad for\ \dfrac{Q}{K} < 1.72$ $r_p = 1.011\, T \exp\left(\dfrac{-41840}{RT}\right) s \exp\left(-\dfrac{2.36}{\ln\left(\dfrac{Q}{K}\right)}\right) \quad for\ \dfrac{Q}{K} > 1.72$	Eq. 3 Eq. 4	Shiraki & Brantley (1995)
Dolomite dissolution rate $r_d = 10^{\left(-0.0436\,pH^2 - 0.5948\,pH - 2.0509\right)} \dfrac{T}{353.15}$ $\left[\exp\left(\dfrac{(972\,pH - 5951)(353.15 - T)}{353.15\,T}\right)\right] s\left(1 - \dfrac{Q}{K}\right)$	Eq. 5	Gautelier et al. (1999)
Dolomite precipitation rate $r_p = 1.122\text{x}10^5 \exp\left(\dfrac{-16060}{T}\right) s \left(\dfrac{Q}{K} - 1\right)^{2.26}$	Eq. 6	Arvidson & Mackenzie (1999)

Reaction rates laws		sources
Quartz dissolution rate $$r_d = \begin{bmatrix} \exp(-10.7)\,T\,\exp\left(\dfrac{-66000}{RT}\right)\theta_{>SiOH} + \\ \exp(4.7)\,T\,\exp\left(\dfrac{-82700}{RT}\right)\left(\theta_{>SiO^-_{tot}}\right) \end{bmatrix}^{1.1} s\left(1-\dfrac{Q}{K}\right)$$ with $$\theta_{>SiOH} = 1.055768 - 4.464707\times10^{-2}\,pH + 1.224392\times10^{-2}\,pH^2 - 1.168033\times10^{-3}\,pH^3$$ $$\theta_{>SiO^-_{tot}} = 1 - \theta_{>SiOH}$$	Eq. 7	Dove & Rimstidt (1994)
Quartz precipitation rate $$r_p = \left[a^2_{H_2O}\,\exp\left(\left(1.174 - 2.028\text{x}10^{-3}\,T - \dfrac{4158}{T}\right)\ln 10\right)\right] s\left(\dfrac{Q}{K}-1\right)$$	Eq. 8	Rimstidt & Barnes (1980)
Pyrite dissolution rate $$r_d = 3.23\text{x}10^6\,\exp(-0.0455\,T)\exp\left(\dfrac{-65000}{RT}\right) s\left(1-\dfrac{Q}{K}\right)$$	Eq. 9	Williamson & Rimstidt (1994)
Pyrite precipitation rate $$r_p = \dfrac{K_{FeS}}{K_{H_2S}}\,a_{Fe}\,a^2_{HS}\left(\dfrac{256.797}{T} - 0.534\right)\exp\left(\dfrac{-34140}{RT}\right) s\left(\dfrac{Q}{K}-1\right)$$	Eq. 10	Rickard (1997) Rickard & Luther (1997)
Amorphous silica dissolution rate $$r_d = 10^{\left(0.82191 - \frac{3892.3}{T}\right)} a_{SiO_2}\,a^2_{H_2O}\,s\left(1-\dfrac{Q}{K}\right)$$	Eq. 11	Rimstidt & Barnes (1980) Icenhower & Dove (2000)
Amorphous silica precipitation rate $$r_p = 3.8\text{x}10^{-10}\,\exp\left(\dfrac{-50000}{R}\left(\dfrac{1}{T} - \dfrac{1}{298.15}\right)\right) s\left(\left(\dfrac{Q}{K}\right)^{4.4} - \dfrac{1}{\left(\dfrac{Q}{K}\right)^{8.8}}\right)$$	Eq. 12	Rimstidt & Barnes (1980) Xu et al. (2004b) Carroll et al. (1998)
K-Feldspar dissolution rate $$r_d = 5.25\text{x}10^{-6}\,\exp\left(\dfrac{-51700}{RT}\right)\left[\dfrac{10^{-0.97}\,a_{H^+}}{1 + 10^{-0.97}\,a_{H^+} + 10^{3.04}\,a_{Na^+}}\right]^{0.5} s\left(1-\dfrac{Q}{K}\right)$$	Eq. 13	Stillings & Brantley (1995) Blum & Stillings (1995)
K-Feldspar precipitation rate $$r_p = 10^{-12}\,\exp\left(\dfrac{-67830}{R}\left(\dfrac{1}{T} - \dfrac{1}{298.15}\right)\right) s\left(\dfrac{Q}{K}-1\right)$$	Eq. 14	Blum & Stillings (1995)
Albite dissolution rate $$r_d = 0.35\,\exp\left(\dfrac{-89000}{RT}\right)\left[\dfrac{10^{-0.97}\,a_{H^+}}{1 + 10^{-0.97}\,a_{H^+} + 10^{3.04}\,a_{Na^+}}\right]^{0.5} s\left(1-\dfrac{Q}{K}\right)$$	Eq. 15	Stillings & Brantley (1995) Hellmann (1994)

Reaction rates laws		sources
Albite precipitation rate $$r_p = 10^{-12} \exp\left(\frac{-67830}{R}\left(\frac{1}{T} - \frac{1}{298.15}\right)\right) s\left(\frac{Q}{K} - 1\right)$$	Eq. 16	Blum & Stillings (1995)
Illite dissolution rate $$r_d = \left[2.2 \times 10^{-4} \exp\left(\frac{-46000}{RT}\right) a_{H^+}^{0.6} + 2.5 \times 10^{-13} \exp\left(\frac{-14000}{RT}\right)\right] s\left(1 - \frac{Q}{K}\right)$$	Eq. 17	Köhler et al. (2003)
Illite precipitation rate $$r_p = 1.1638\, T \exp\left(\frac{-117000}{RT}\right) s\left(\frac{Q}{K} - 1\right)^2$$	Eq. 18	Nagy et al. (1991)

[*] R is the gas constant (= 8.314 J mol^{-1} K^{-1}) and T the temperature in Kelvin

4.2 TOUGHREACT

Equation 1 (TST kinetic rate law) is implemented into TOUGHREACT in a generic form, and rate parameters are input into the model for each mineral. The variation of the rate constant with temperature is implemented through the Arrhenius equation:

$$k = k_{298.15} \exp\left[\frac{-E_a}{R}\left(\frac{1}{T} - \frac{1}{298.15}\right)\right]$$
Eq. 19

where E_a is the activation energy, $k_{298.15}$ is the rate constant at 25°C, R is the gas constant and T is the absolute temperature in Kelvin. Equation 19 does not consider pH effects, and is generally applied at neutral pH (neutral mechanism). Because dissolution and precipitation processes can be affected by H$^+$ (acid mechanism) or OH$^-$ (base mechanism), the full rate law expression for these cases is implemented as

$$k = k_{25}^{nu} \exp\left[\frac{-E_a^{nu}}{R}\left(\frac{1}{T} - \frac{1}{298.15}\right)\right] + k_{25}^{ac} \exp\left[\frac{-E_a^{ac}}{R}\left(\frac{1}{T} - \frac{1}{298.15}\right)\right] a_{H^+}^{n_{ac}}$$
$$+ k_{25}^{ba} \exp\left[\frac{-E_a^{ba}}{R}\left(\frac{1}{T} - \frac{1}{298.15}\right)\right] a_{H^+}^{n_{ba}}$$
Eq. 20

where the subscripts *nu*, *ac* and *ba* indicate neutral, acid and base mechanisms, respectively and a_{H+} is the activity of hydrogen ion. The values of the different parameters have been compiled for many minerals by Palandri and Kharaka (2004), using the data sources shown in Table 4-2.

Table 4-2. Mineral dissolution rate parameters used in TOUGHREACT simulations. Parameters for the neutral mechanism are also used to describe mineral precipitation rates.

	Acid mechanism				Neutral mechanism			Base mechanism		
	Log k	E	n	m	Log k	E	p	Log k	E	n
Calcite[1]	-0.30	14.4	1.000	--	-5.81	23.5	--	-3.48	35.4	1.000
Sedimentary dolomite[2]	-3.19	36.1	0.500	--	-7.53	52.2	--	-5.11	34.8	0.500
Hydrothermal dolomite[2]	-3.76	56.7	0.500	--	-8.60	95.3	--	-5.37	45.7	0.500
Pyrite[3]	-7.52	56.9	-0.500	0.500	-4.55	56.9	0.500	--	--	--
Quartz[4]	--	--	--	--	-13.99	87.7	--	--	--	--
Amorphous silica[4]	--	--	--	--	-12.14	62.9	--	--	--	--
K-feldspar[5]	-10.06	51.7	0.500	--	-12.41	38.0	--	-21.20	94.1	-0.823
Albite[6]	-10.16	65.0	0.457	--	-12.56	69.8	--	-15.60	71.0	-0.572
Illite[7]	-10.98	23.6	0.340	--	-12.78	35.0	--	-16.52	58.9	-0.400

Log_{10} rate constant k fitted to Eq. 20 at 25°C (assuming $a_{H+} = 1$) expressed in mol m^{-2} s^{-1} (Palandri and Kharaka, 2004)

E = Arrhenius activation energy (kJ.mol^{-1})

n = Reaction order with respect to H^+

m = Reaction order with respect to Fe^{+++}

p = Reaction order with respect to O_2

[1] Plummer et al. (1978) and Talman et al. (1990); [2]Busenberg and Plummer (1982); [3]McKibben and Barnes (1986); [4]Icenhower and Dove (2000); [5]Blum and Stillings (1995), Helgeson et al. (1984), Bevan and Savage (1989), Gautier et al. (1994), and Knauss and Copenhaver (1995); [6]Chou and Wollast (1985), Hellman (1994); [7]Bauer and Berger (1998), Huertas et al. (2001), Sverdrup (1990) and Zysset and Schindler (1996).

4.3 COMPARISON AND INTERPRETATION

As presented above, FRACHEM and TOUGHREACT make use of TST-type rate laws, but these laws do not take exactly the same form in both codes. Most often, the rate laws and parameters implemented into FRACHEM were established specifically for high-salinity and/or high-temperature fluids most relevant to the reservoir conditions at Soultz. Rate laws for all minerals incorporate a dependence on temperature. Other specific dependencies are implemented for certain minerals. For the carbonates, the dissolution equation depends on pH, whereas for quartz, we note the influence of salinity through the water activity. For the feldspars group, dissolution rates are a function of Na^+, which plays an inhibitor role in the dissolution of these minerals (Stillings and Brantley, 1995). In TOUGHREACT, one generic equation is used incorporating different mechanisms which are activated or not depending on the mineral considered. In this study, no dependencies on the concentration of species other than H^+ (Equation 20) are applied (Table 4-2).

Rates computed according to these different rate laws as a function of temperature are compared in Figures 4-1 through 4-8, and discussed in separate subsections below. The comparisons were done for pH 5, assuming unit surface areas and no limitation from the affinity term (i.e., [1– Q/K] ≈ 1). Concentrations of species required in some rate laws were fixed at values representative of field conditions, as discussed below. For each mineral, both the precipitation and dissolution rates are shown on the same plot, using opposite directions on the Y axis. The FRACHEM

results are shown by continuous lines; the TOUGHREACT results are displayed with dashed lines.

4.3.1 Calcite – Quartz – Amorphous silica

For these three minerals, the two codes give results that are in fairly good agreement (Figures 4-1, 4-2 and 4-3). The differences in rates do not exceed 1.5 orders of magnitude, except for the case of the calcite precipitation rate if a saturation index exceeding 1.72 is supposed. In this case, an alternative precipitation rate is applied with FRACHEM (Eq. 4, Table 4-1), yielding a rate about 3 orders of magnitude larger (Figure 4-1) than when the saturation index is < 1.72.

Figure 4-1.   Calcite precipitation rate (bottom) and dissolution rate (top) at pH 5 (see text).

Figure 4-2.   Quartz precipitation rate (bottom) and dissolution rate (top) at pH 5 (see text).
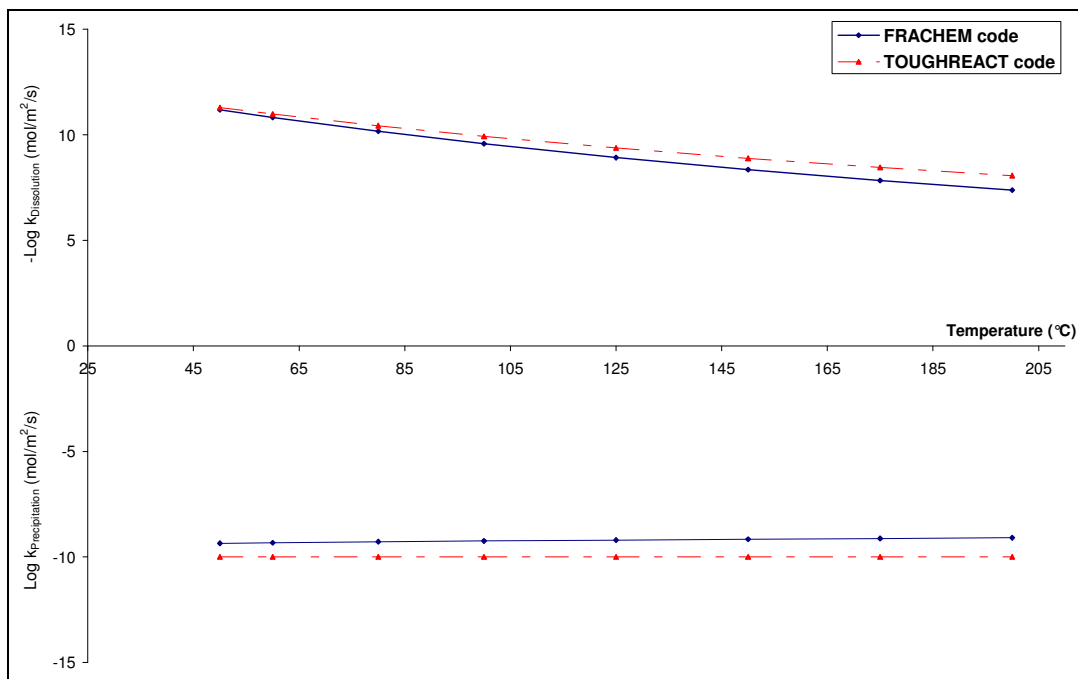
Figure 4-3.   Amorphous silica precipitation rate (bottom) and dissolution rate (top) at pH 5 (see text).

4.3.2 Aluminosilicates

For K-feldspar (Figure 4-4) the precipitation and dissolution rates computed by both codes differ by 2–3 orders of magnitude. This difference is explained in part by the different activation energies used in the two codes (67.83 kJ.mol^{-1} with FRACHEM and 38 kJ.mol^{-1} with TOUGHREACT). The albite precipitation rates are in good agreement (Figure 4-5); however, the albite dissolution rates differ by about 2 orders of magnitude. This discrepancy can be explained by the fact that, with FRACHEM, the inhibitor effect of Na$^+$ is taken into consideration (concentration of 1.2 molal assumed here), whereas it is not with TOUGHREACT. Differences in pH dependence also affect model results. For illite (Figure 4-6), similar differences around 2–3 orders of magnitude are mainly caused by differences in activation energies, as well as in the exponent applied to H$^+$ activity (0.6 with FRACHEM, 0.34 with TOUGHREACT).
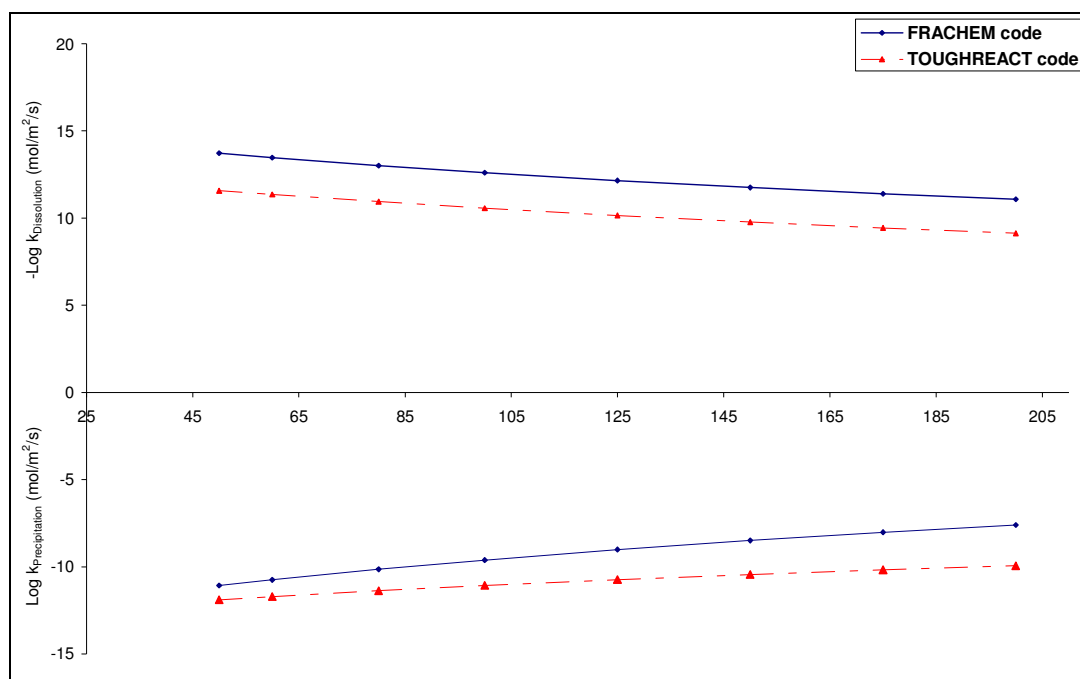
Figure 4-4. K-feldspar precipitation rate (bottom) and dissolution rate (top) at pH 5 (see text).
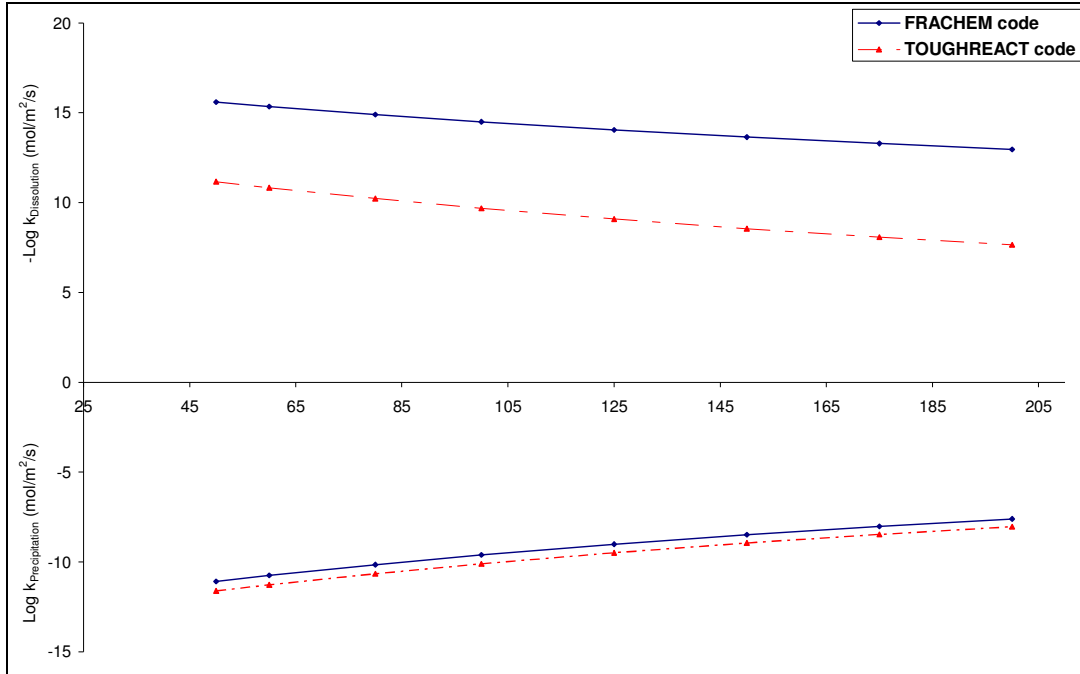
Figure 4-5.   Albite precipitation rate (bottom) and dissolution rate (top) at pH 5 and Na$^+$ concentration of 1.2 molal (see text).
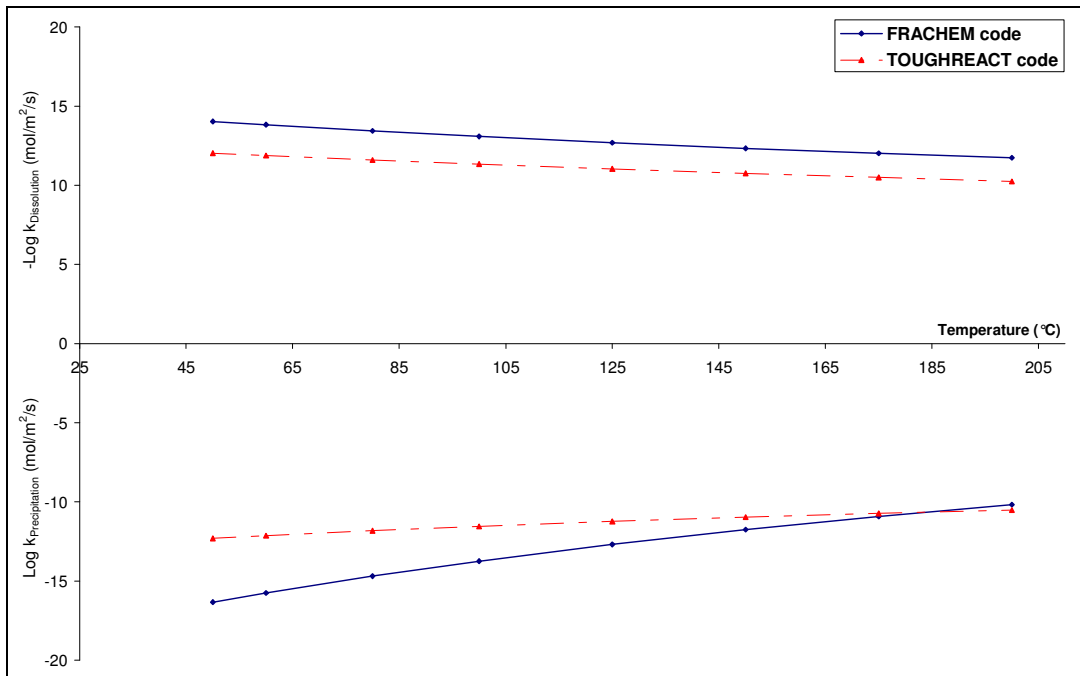
Figure 4-6.   Illite precipitation rate (bottom) and dissolution rate (top) at pH 5 (see text).

4.3.3 Dolomite – Pyrite

These two minerals show the most marked differences. For dolomite, the spread between models can reach 4 and 10 orders of magnitude, for dissolution and precipitation, respectively, regardless of the type of dolomite considered (hydrothermal or sedimentary, Table 4-2). The dolomite dissolution-rate parameters used in FRACHEM were extrapolated from experimental results reported by Gautelier et al. (1999) at pH -0.39 to 4.4 and temperatures between 25 and 80°C. The dissolution rates obtained with these parameters are in good agreement with the TOUGHREACT results at low temperatures (Figure 4-7). However, large differences appear at high temperatures, which seems to indicate an inappropriate extrapolation method. The very large differences in precipitation rates are more puzzling. The dolomite precipitation-rate law implemented in FRACHEM comes from Arvidson and Mackenzie (1999), who experimentally determined rates between 100 and 200°C and for pH ranging from 4.8 to 7. Nevertheless, the accuracy of this rate is apparently questionable because of dolomite precipitation competing with magnesian calcite formation. This could explain why this reaction rate was quite underestimated when compared to the rates used with TOUGHREACT.

Dissolution and precipitation reactions of pyrite (Figure 4-8) are governed by many processes and factors including pH, O_2/sulfide levels and Fe^{++} concentration. The pyrite precipitation rate law implemented into FRACHEM (Table 4-1) incorporates HS^- and Fe^{++} concentrations (assumed here at 1 and 2.5 millimolal at pH 5, respectively), whereas a simpler rate law is applied for dissolution (Table 4-1). In contrast, the rate law used with TOUGHREACT (McKibben and Barnes, 1986) is the same for precipitation and dissolution, and was determined for pyrite dissolution at pH 1–2 and temperature of 30°C.
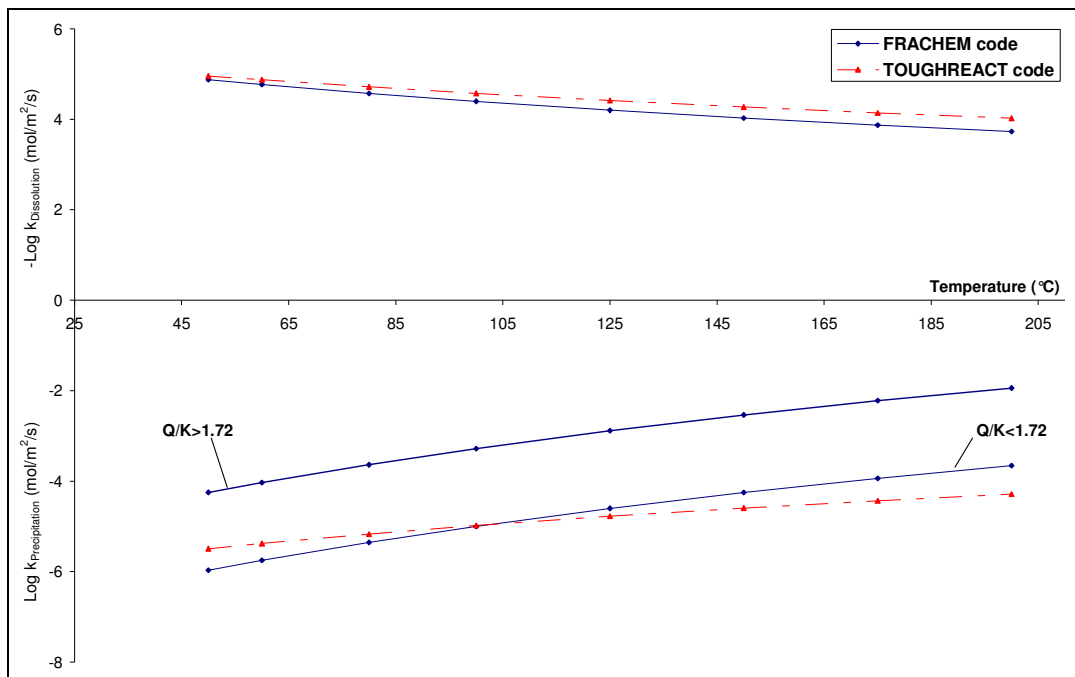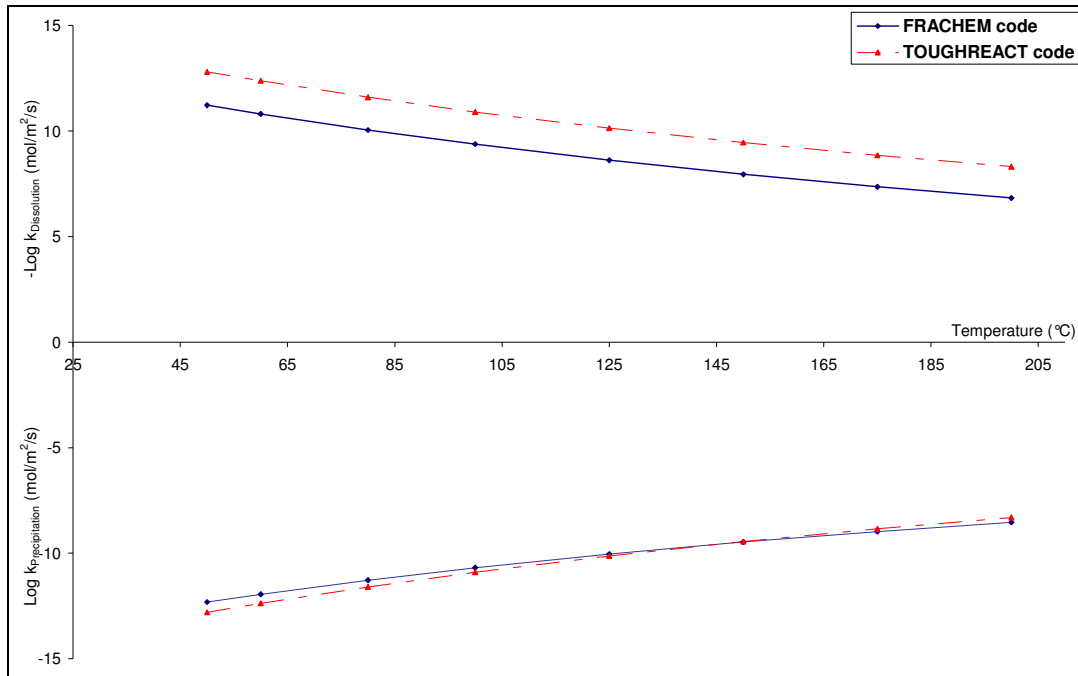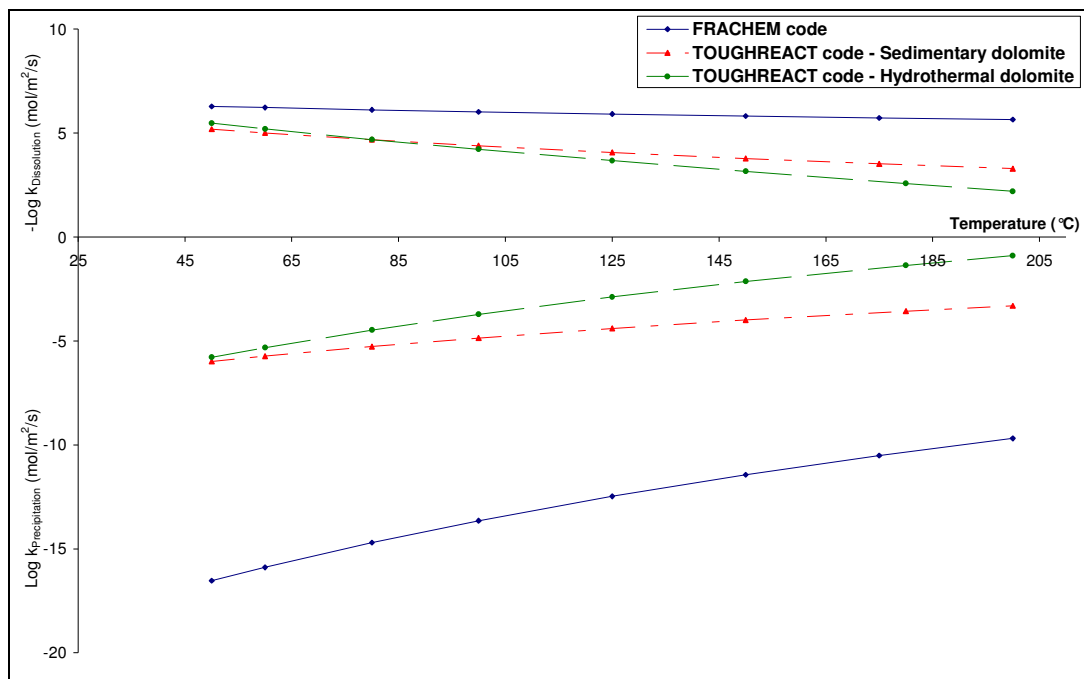

Figure 4-7. Dolomite precipitation rate (bottom) and dissolution rate (top) at pH 5 (see text).
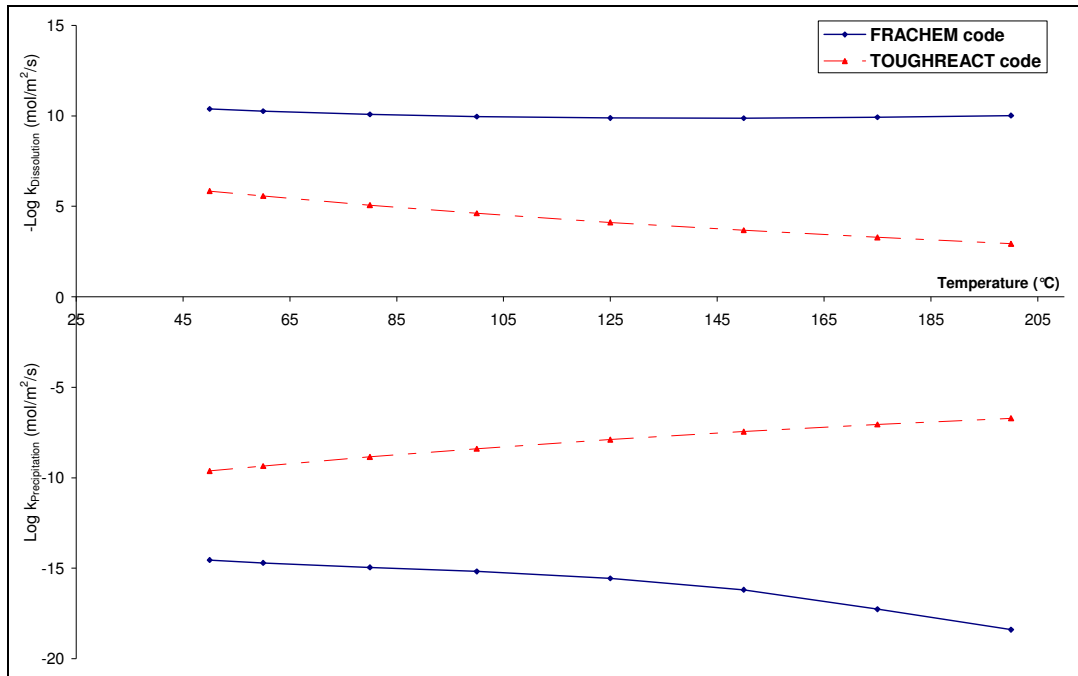
Figure 4-8.   Pyrite precipitation rate (bottom) and dissolution rate (top) at pH 5, 2.5x10^{-3} molal Fe^{++}, and 10^{-3} molal HS^{-} (see text).

.

5   EQUILIBRIUM CONSTANTS

In this section, we compare the equilibrium constants used in the FRACHEM and TOUGHREACT simulations. It should be recalled here that for the case of TOUGHREACT, these equilibrium constants are read from a separate (code-independent) thermodynamic database. Comparisons of all thermodynamic data in this database with corresponding data implemented into FRACHEM are beyond the scope of this study. For this reason, only data for key minerals are compared here. The full TOUGHREACT database used in the present study (*thermXu4-ns.dat*) consists primarily of equilibrium constants derived using SUPCRT92 (Johnson et al., 1992) with input thermodynamic properties in the SUPCRT92 database *sprons96.dat*.   Essentially the same data are used in FRACHEM, except as discussed below. One main difference between the codes is that the effect of pressure on equilibrium constants is explicitly taken into account with FRACHEM. With TOUGHREACT, the thermodynamic database is created for a given pressure (or pressure curve), and only the temperature effect is considered in the course of a simulation. In the present case, the thermodynamic data were derived for pressures along the water-pressure saturation curve at temperatures above 100°C, and at 1 bar at temperatures below 100°C. The equilibrium constants input into FRACHEM were initially computed along the same water-saturation pressure curve, however, these constants are recomputed with changes in pressure during run time as discussed further below.

5.1   COMPARISONS FOR SELECTED MINERALS

Equilibrium constants (as log(K) values) for key minerals are compared in Table 5-1. For each mineral, the first record in this table corresponds to the reactants (negative stoichiometric coefficients) and products (positive stoichiometric coefficients) of the mineral dissolution reaction. The second and third records give the logarithmic values (base 10) of the equilibrium constants used with FRACHEM and TOUGHREACT, respectively, for the dissolution reaction shown. Data sources are also included in Table 5-1.

It should be noted that, in the TOUGHREACT database, aqueous silica is considered in the form of $SiO_{2(aq)}$. With FRACHEM, it is considered in the form of H_4SiO_4. By convention, the log(K) for the reaction $H_4SiO_4 = 2H_2O + SiO_{2(aq)}$ is zero, such that the log(K) values for quartz and amorphous silica reported in Table 5-1 for both codes correspond to equivalent (effectively the same) reactions.

The equilibrium constants of aluminium silicate minerals in the TOUGHREACT database are expressed in terms of AlO_2^- and $SiO_{2(aq)}$, whereas reactions in terms of Al^{3+} and H_4SiO_4 are used in FRACHEM. To better compare the equilibrium constants between both codes, we converted the TOUGHREACT data to reactions in terms of Al^{3+} and H_4SiO_4, using the convention discussed above for silica and log(K) data used by TOUGHREACT for the reaction $Al^{3+} + 2H_2O = 4H^+ + AlO_2^-$ (from SUPCRT92).

Table 5-1. Comparison of equilibrium constant values for selected minerals used in FRACHEM and TOUGHREACT simulations. The dissolution reaction is placed in front of each mineral, with negative coefficients corresponding to the reactants, and positive coefficients corresponding to products. The calculations are made at 1 bar up to 100 °C, and at saturation vapor pressure for T > 100 °C.

Temperature (°C)	0	25	60	100	150	200	250
Calcite	$-1.00\ H^+$	$1.00\ Ca^{2+}$	$1.00\ HCO_3^-$				
Log K (FRACHEM)[a]	2.227	1.847	1.334	0.775	0.099	-0.583	-1.326
Log K (TREACT)[a]	2.226	1.849	1.333	0.774	0.100	-0.584	-1.326
Dolomite	$-2.00\ H^+$	$1.00\ Ca^{2+}$	$1.00\ Mg^{2+}$	$2.00\ HCO_3^-$			
Log K (FRACHEM)[a]	3.408	2.509	1.334	0.095	-1.351	-2.773	-4.297
Log K (TREACT)[a]	3.406	2.514	1.331	0.094	-1.349	-2.774	-4.297
Quartz	$-2.00\ H_2O$	$1.00\ H_4SiO_4$					
Log K (FRACHEM)[b]	-4.501	-4.001	-3.500	-3.097	-2.717	-2.427	-2.312
Log K (TREACT)[a,e]	-4.079	-3.739	-3.349	-2.992	-2.642	-2.365	-2.206
Amorphous silica	$-2.00\ H_2O$	$1.00\ H_4SiO_4$					
Log K (FRACHEM)[c]	-2.967	-2.738	-2.465	-2.215	-1.979	-1.813	-1.700
Log K (TREACT)[a,e]	-3.124	-2.714	-2.407	-2.184	-1.98	-1.819	-1.693
Pyrite	$-1.00\ H_2O$	$1.00\ Fe^{2+}$	$1.75\ HS^-$	$0.25\ H^+$	$0.25\ SO_4^{2-}$		
Log K (FRACHEM)[a]	-26.500	-24.656	-22.748	-21.238	-20.019	-19.428	-19.694
Log K (TREACT)[a,f]	-26.504	-24.653	-22.753	-21.235	-20.024	-19.396	-19.278
K-feldspar	$-4.00\ H_2O$	$-4.00\ H^+$	$1.00\ K^+$	$1.00\ Al^{3+}$	$3.00\ H_4SiO_4$		
Log K (FRACHEM)[d]	0.455	0.068	-0.503	-1.105	-1.701	-2.154	-2.651
Log K (TREACT)[a,g]	0.934	-0.027	-1.048	-1.944	-2.873	-3.745	-4.574
Albite (High temperature)	$-4.00\ H_2O$	$-4.00\ H^+$	$1.00\ Na^+$	$1.00\ Al^{3+}$	$3.00\ H_4SiO_4$		
Log K (FRACHEM)[d]	5.416	4.405	3.118	1.878	0.685	-0.211	-1.052
Log K (TREACT)[a,g]	3.731	3.228	2.038	0.7	-0.722	-1.902	-2.939
Illite	$-8.00\ H^+$	$-2.00\ H_2O$	$0.60\ K^+$	$2.30\ Al^{3+}$	$0.25\ Mg^{2+}$	$3.50\ H_4SiO_4$	
Log K (FRACHEM)[d]	13.450	10.340	6.850	3.820	0.810	-1.230	-2.870
Log K (TREACT)[a,g]	11.386	9.026	5.555	2.047	-1.59	-4.612	-7.253

[a]SUPCRT92 (Johnston et al., 1992); [b]Walther & Helgeson (1977); [c]Gunnarsson and Arnorson (2000); [d]Helgeson et al. (1978); [e]Originally expressed in terms of $SiO_{2(aq)}$ instead of H_4SiO_4, see text; [f]Converted from original reaction in terms of $O_{2(aq)}$ using the log(K) data for the reaction $HS^- + 2O_{2(aq)} = H^+ + SO_4^{2-}$ in the same database (from SUPCRT92); [g]Converted from original reaction in terms of AlO_2^- and $SiO_{2(aq)}$ as discussed in text.

5.2   REMARKS

A reasonably good agreement is observed between the log(K) values used here with FRACHEM and TOUGHREACT for carbonates (calcite and dolomite) and silica phases (quartz and amorphous silica). The differences in quartz solubilities reflect more recent data implemented in FRACHEM consistent with new measurements by Rimstidt (1997). Significant divergences appear with aluminosilicates. Note that log(K) values for reactions expressed in terms of $Al(OH)_3$ or $Al(OH)_4^-$ (also corresponding to $HAlO_2$ and AlO_2^-, respectively) instead of Al^{3+} would yield smaller differences, because differences in the first hydrolysis constant of Al^{3+} reported in the literature are larger than for the second and higher hydrolysis constants. It should also be noted that in the Soultz fluids considered here (pH 4.5 to 5.5 range), Al^{3+} dominates the aluminium species only at temperatures below about 100°C. At temperatures above 100°C, the other two complexes start to dominate.

5.3   VARIATION OF MINERAL SOLUBILITY WITH PRESSURE

In the Soultz reservoir, at a depth of 5,000 m, the pressure is estimated to be about 500 bar. Under these conditions, pressure plays a significant role in mineral solubility, particularly for the carbonates, as discussed below.

The pressure effect on the solubility of minerals has been implemented in FRACHEM for some minerals. The effect of pressure (P) on the solubility of minerals in water can be estimated from:

$$\ln\left(\frac{K_{P,T}}{K_{P_0,T}}\right) = \left(\frac{-P\Delta V + 0.5\Delta\kappa P^2}{RT}\right) \qquad \text{Eq. 21}$$

where K is the equilibrium constant, P_0 is the reference pressure (here taken as 1 bar below 100°C and the water saturation pressure above 100°C), R is the gas constant (83.15 cm^3 bar K^{-1} mol^{-1}) and T is the absolute temperature (°K). The volume (ΔV) and compressibility ($\Delta\kappa$) changes at atmospheric pressure are given by:

$$\Delta V = \sum \overline{V_i}(products) - \sum \overline{V_i}(reactants)$$
$$\Delta\kappa = \sum \overline{\kappa_i}(products) - \sum \overline{\kappa_i}(reactants)$$

V_i and κ_i are the partial volume and compressibility of species i. Standard partial molar volume of aqueous cations and anions at vapor-liquid saturation pressures for H_2O and temperature from 0° to 350 °C are given by Millero (1982) and Tanger and Helgeson (1988).

The variations in solubility products of calcite (Table 5-2) and dolomite (Table 5-3) were estimated between 1 and 1000 bars using Equation 21. The effect of pressure on equilibrium constants for these minerals is quite important, showing significant solubility increase with pressure at all temperatures. From these data, the following two correlations were established with temperature T in °C, and pressure P in bar:

- For calcite:

$$K_{T,P} = K_{T,P_0} \exp\left[-\left(\frac{-1.5155\times10^{-3}T^2 + 0.1811T - 34.477}{83.14(273.15+T)}\right)P\right]$$ Eq. 22

- For dolomite:

$$K_{T,P} = K_{T,P_0} \exp\left[-\left(\frac{-3.0751\times10^{-3}T^2 + 0.3405T - 62.0860}{83.14(273.15+T)}\right)P\right]$$ Eq. 23

Table 5-2.   Evolution of $K_{T,P}/K_{T,P0}$ with temperature and pressure for calcite.

Temperature (°C)	Pressure (bars)									
	100	200	300	400	500	600	700	800	900	1000
0	1.159	1.337	1.534	1.750	1.986	2.240	2.514	2.805	3.112	3.433
10	1.145	1.307	1.483	1.676	1.883	2.107	2.344	2.596	2.861	3.136
25	1.127	1.266	1.416	1.577	1.750	1.933	2.127	2.330	2.542	2.762
50	1.113	1.236	1.368	1.510	1.662	1.823	1.993	2.172	2.360	2.557
75	1.107	1.224	1.350	1.485	1.630	1.785	1.951	2.126	2.312	2.508
100	1.106	1.223	1.349	1.486	1.634	1.793	1.964	2.147	2.343	2.553
125	1.110	1.232	1.365	1.511	1.669	1.842	2.029	2.232	2.452	2.689
150	1.120	1.253	1.401	1.564	1.745	1.943	2.161	2.401	2.664	2.952
175	1.139	1.297	1.476	1.677	1.903	2.158	2.443	2.763	3.120	3.520
200	1.161	1.347	1.562	1.809	2.092	2.417	2.789	3.214	3.699	4.252

Table 5-3.   Evolution of $K_{T,P}/K_{T,P0}$ with temperature and pressure for dolomite.

Temperature (°C)	Pressure (bars)									
	100	200	300	400	500	600	700	800	900	1000
0	1.302	1.685	2.160	2.745	3.456	4.313	5.334	6.536	7.938	9.553
10	1.276	1.619	2.036	2.540	3.142	3.853	4.686	5.652	6.759	8.015
25	1.240	1.529	1.871	2.272	2.738	3.275	3.888	4.580	5.354	6.212
50	1.214	1.468	1.762	2.103	2.492	2.935	3.434	3.991	4.610	5.289
75	1.205	1.446	1.726	2.048	2.416	2.835	3.307	3.837	4.425	5.075
10	1.206	1.450	1.735	2.066	2.446	2.882	3.379	3.942	4.574	5.282
125	1.218	1.480	1.789	2.154	2.580	3.077	3.652	4.315	5.074	5.940
150	1.242	1.539	1.899	2.334	2.855	3.477	4.217	5.092	6.122	7.328
175	1.290	1.662	2.132	2.723	3.465	4.389	5.537	6.957	8.703	10.843
200	1.344	1.804	2.412	3.212	4.259	5.624	7.397	9.688	12.638	16.419

The variations in the solubility of quartz with pressure (Table 5-4) are given by Fritz (1981), whereas Fournier and Rowe (1977) presents the variation of solubility of amorphous silica in water at high temperatures and an elevated pressure of 1034 bar (Table 5-5). As shown by these data, the solubility increase in quartz and amorphous silica with pressure is not negligible, although it is much less than for the carbonates.

Table 5-4.　Solubility of quartz (mg SiO_2/kg water) as a function of temperature and pressure.

T (°C)	0	25	50	100	150	200	250	300
P_{sat}	1 bar	1 bar	1 bar	1 bar	4.8 bar	15.5 bar	39.7 bar	85.8 bar
	1.89	6.00	12.2	48.3	115	225	384	586
500 bars	1.97	7.12	17.5	60.6	144	278	473	730
1000 bars	1.99	8.20	21.0	74.6	177	340	576	895

Table 5-5.　Change in amorphous silica equilibrium constant with pressure.

T(°C)	25	50	75	100	125	150	175	200
$K_{T,1034}/K_{T,1}$	1.084	1.136	1.183	1.225	1.263	1.298	1.330	1.358

$K_{T,1034}$ and $K_{T,1}$ refer to the values of amorphous silica solubility at 1034 and 1 bar, respectively.

From these data, the following two correlations were established with temperature T in °C, and pressure P in bar:

- For quartz:

$$K(T,P) = K(T,P_0)\exp\left[\begin{matrix} 7\times10^{-10}T^4 - 5.25\times10^{-7}T^3 + 1.45\times10^{-4}T^2 \\ -1.74\times10^{-2}T + 5.74\times10^{-4}P + 1.713 \end{matrix}\right]$$

Eq. 24

- For amorphous silica:

$$\frac{K_{T,1034\,bar}}{K_{T,P_{sat}}} = 10^{-\frac{79}{T}+0.3}$$

Eq. 25

To gain confidence in the correlations established above, the equilibrium constants calculated with FRACHEM using Equations 22 to 25 were compared with values computed directly with SUPCRT92 (Johnston et al., 1992).　The results (Table 5-6) show reasonably good agreement.

Table 5-6: Comparison of the equilibrium constants computed with FRACHEM and SUPCRT92 as a function of temperature and pressure

Temperature (°C)		0	25	50	100	150	200	250
Calcite	Log K (FRACHEM) – 500 bars	2.555	2.117	1.715	1.000	0.365	-0.241	-0.883
	Log K (SUPCRT) – 500 bars	2.535	2.100	1.701	0.979	0.314	-0.334	-0.997
	Log K (FRACHEM) – 1000 bars	2.883	2.386	1.942	1.226	0.631	0.101	-0.440
	Log K (SUPCRT) – 1000 bars	2.797	2.317	1.896	1.158	0.498	-0.125	-0.738
Dolomite	Log K (FRACHEM) – 500 bars	4.001	2.995	2.087	0.506	-0.856	-2.127	-3.453
	Log K (SUPCRT) – 500 bars	3.955	2.962	2.062	0.473	-0.942	-2.285	-3.638
	Log K (FRACHEM) – 1000 bars	4.595	3.481	2.513	0.918	-0.361	-1.481	-2.608
	Log K (SUPCRT) – 1000 bars	4.406	3.339	2.404	0.793	-0.602	-1.886	-3.128
Quartz	Log K (FRACHEM) – 500 bars	-4.200	-3.683	-3.138	-2.621	-2.132	-1.753	-1.565
	Log K (SUPCRT) – 500 bars	-3.966	-3.367	-3.011	-2.571	-2.279	-2.052	-1.872
	Log K (FRACHEM) – 1000 bars	-4.142	-3.627	-3.087	-2.581	-2.101	-1.728	-1.543
	Log K (SUPCRT) – 1000 bars	-3.919	-3.290	-2.924	-2.482	-2.194	1.970	-1.782
Amorphous Silica	Log K (FRACHEM) – 1000 bars	-2.956	-2.703	-2.410	-2.127	-1.866	-1.680	-1.551
	Log K (SUPCRT) – 1000 bars	-2.959	-2.497	-2.250	-1.960	-1.769	-1.621	-1.504

6 APPLICATION – SIMULATION OF INJECTION

6.1 MODEL CONCEPTUALISATION AND INPUT DATA

The two codes were applied to a geometrical model representing the granitic reservoir in Soultz. Injection and production wells were linked by fractures zones surrounded by a low-permeability granite matrix. The model is composed of 1,250 fractured zones. Each fracture zone has an aperture of 0.1 m, a fixed horizontal depth of 10 m, and a porosity of 10%. Here, reactive transport is simulated into one of these fractured zones, with the assumption that the fluid exchange with the surrounding low-permeability matrix is insignificant. Due to the symmetrical shape of the geometrical model, only the upper half of the fractured zone is considered in the simulation. It should be noted that, with FRACHEM, matrix gridblocks are added above the fracture blocks for proper thermal behavior. The area is discretized into 222 two-dimensional gridblocks (Figure 6-1): 25 for the fracture zone and 197 for the matrix. The size of the gridblocks ranges from a minimum of 0.5 m x 0.05 m near the injection and the production wells to a maximum of 50 m x 35 m. With TOUGHREACT, however, only the fracture zone is modeled, without adjacent matrix gridblocks. Heat loss in the impermeable matrix is modeled by a semi-analytical solution (Vinsome and Westerveld, 1980) built into the code. As a result, the model contains only 25 gridblocks.
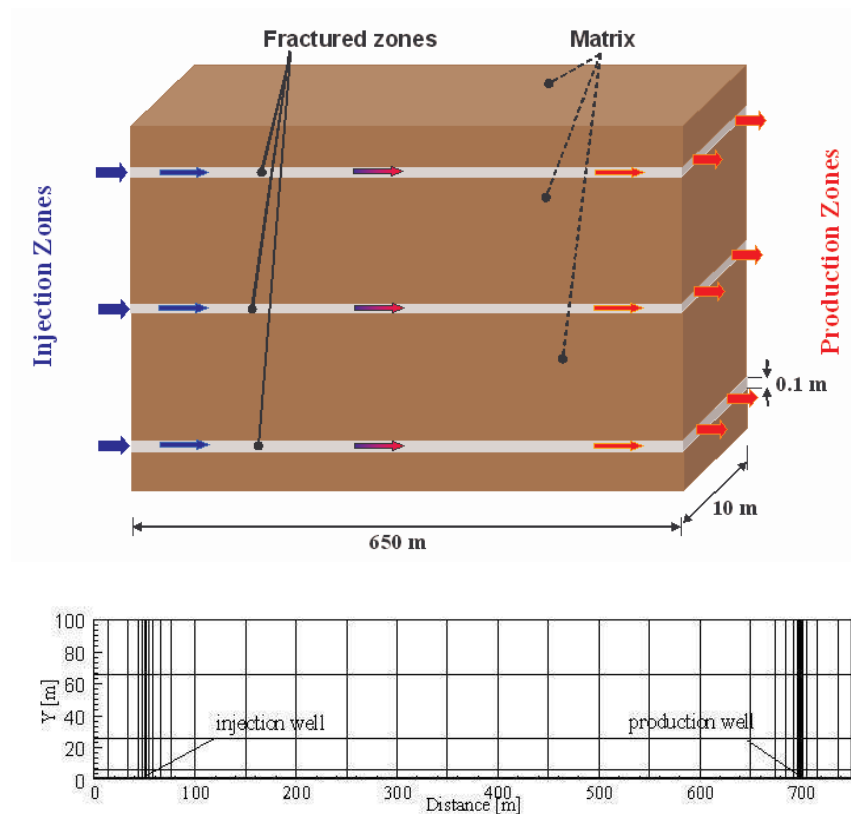

Figure 6-1:   Simplified model and spatial discretization.

Initially, the system temperature was set to the reservoir temperature of 200°C. The geothermal fluid (Table 3-1) was injected in the modeled fractured zone at a rate of 2×10^{-2} L s^{-1} (corresponding to a total production rate of 50 L s^{-1} for the full geometric model) and constant temperature of 65°C. During this simulation, a constant overpressure of 8 MPa was assumed at the injection well, and a hydrostatic pressure was assumed at the production well. With FRACHEM, Dirichlet boundary conditions were applied to the upper, left, and right side of the model. The fluid was continuously recirculated from the production well to the injection well. With TOUGHREACT, the fluid was not recirculated (continuous injection of the same fluid composition), and constant boundary conditions were simulated by connecting gridblocks of infinite dimensions to the injection well (constant chemical composition, temperature, and pressure) and to the production well (constant temperature and pressure).

The values of thermal and hydrological parameters considered in the simulation are listed in Table 6-1. The assumed initial fluid composition is the same as that used for the cooling simulations presented in Section 3 (Table 3-1). However, in this case, the pH of the initial fluid was adjusted to reflect equilibrium of this fluid with calcite in all simulations (i.e., FRACHEM, Tr-DH, and Tr-Pitzer). In this way, simulations with the three codes reflected the same model conceptualization, i.e., that the reservoir fluid is at equilibrium with calcite, which is anticipated to be the case in the field. Making this same assumption for all three models also resulted in minimizing differences in model results caused by the differences in calcite solubilities computed using the different activity coefficient models (see Section 3). The initial fluid pH computed with the three codes, assuming saturation with respect to calcite, was 4.95 using FRACHEM, 4.76 using Tr-Pitzer, and 5.24 using Tr-DH.

The following minerals were included in the simulation: dolomite, calcite, quartz and potassium feldspar. These minerals are the main phases observed in the reservoir rocks at Soultz. Secondary precipitation of amorphous silica was initially considered. However, because silica concentrations remained below the solubility of amorphous silica in the temperature range considered, amorphous silica was not included in the final simulations. Input kinetic and thermodynamic data were discussed in Sections 4 and 5, respectively. A sequential non-iterative approach (SNIA) to reactive transport was implemented. Owing to the sensitivity of the SNIA method on the time discretization, the time step used for the simulations was limited to 10^2 s.

Table 6-1.   Thermohydraulic model parameters.

Parameters		Fracture	Matrix	Fluid
Permeability	[m^2]	5 10^{-13}	10^{-18}	-
Thermal conductivity	[W/m K]	2.9	3	0.6
Density	[kg/m^3]	-	2650	1000
Heat capacity	[J/kg K]	-	1000	4200
Porosity	[%]	10	2	-

6.2   SIMULATIONS WITH FRACHEM

The observation of the mineral behavior (Figure 6-2) shows that all the reactions occur in the first 20 m of the injection zone. Calcite, a secondary mineral present within granite fractures in relatively small proportions, is the most reactive. In the vicinity of the injection well, calcite dissolves, whereas it precipitates from about 2 to 20 m, because of the retrograde solubility of

calcite (solubility decrease with temperature increase). At the onset of fluid circulation within the reservoir, calcite dissolves mainly within the first two meters of the injection well. This dissolution releases calcium in solution, which is then available for calcite precipitation further away from the injection well, where the temperature increases. With increasing simulation times and decreasing rock temperatures, the dissolution of calcite extends towards the production well and ends when this mineral becomes depleted.

Figure 6-2 shows that dolomite dissolves within the first ten meters from the injection well. Similarly to calcite, dolomite dissolution stops when this mineral becomes depleted. Among silicates, quartz and K-feldspar are major minerals in granite. Contrary to calcite, the solubility of these minerals decreases with cooling. As a consequence, these minerals precipitate near the injection well, but less so further away as temperature increases. As mentioned earlier, the fluid always remains undersaturated with respect to amorphous silica. After 25–30 m along the fracture, the fluid becomes essentially unreactive with all the minerals shown in Figure 6-2 because the injected brine becomes close to equilibrium with these minerals.

Figure 6-2. Evolution of the rock composition in the fracture zone (volume %) after 5 years of circulation simulated with FRACHEM. The dashed lines correspond to initial concentrations.

6.3   SIMULATIONS WITH TR-DH

The carbonates are the most reactive minerals. As presented in the case of the FRACHEM simulation, calcite and dolomite dissolve near the injection well (Figure 6-3). These minerals are predicted to dissolve faster than in the FRACHEM simulations because of small differences in reaction rates. Calcite dissolves for the first 10 m (when temperature is below 145°C), then precipitates between 10 and 100 m from the injection well. Dolomite dissolves within the first 100 m and remains unaffected further out. Quartz precipitation is negligible, whereas feldspars precipitate in the close vicinity of the injection well.

6.4 SIMULATIONS WITH TR-PITZER

The predicted behavior of quartz, K-feldspars and carbonates (calcite, dolomite) is similar to the behavior predicted with FRACHEM and Tr-DH. As shown in Figure 6-4, calcite dissolution is predicted along the fracture zone in the first 3 m from the injection well, and then significant precipitation is predicted further away from the injection well, between 5 and 200 m.

Figure 6-3. Evolution of the rock composition in the porous zone after 5 years of circulation simulated with Tr-DH. The dashed lines correspond to the initial concentrations.
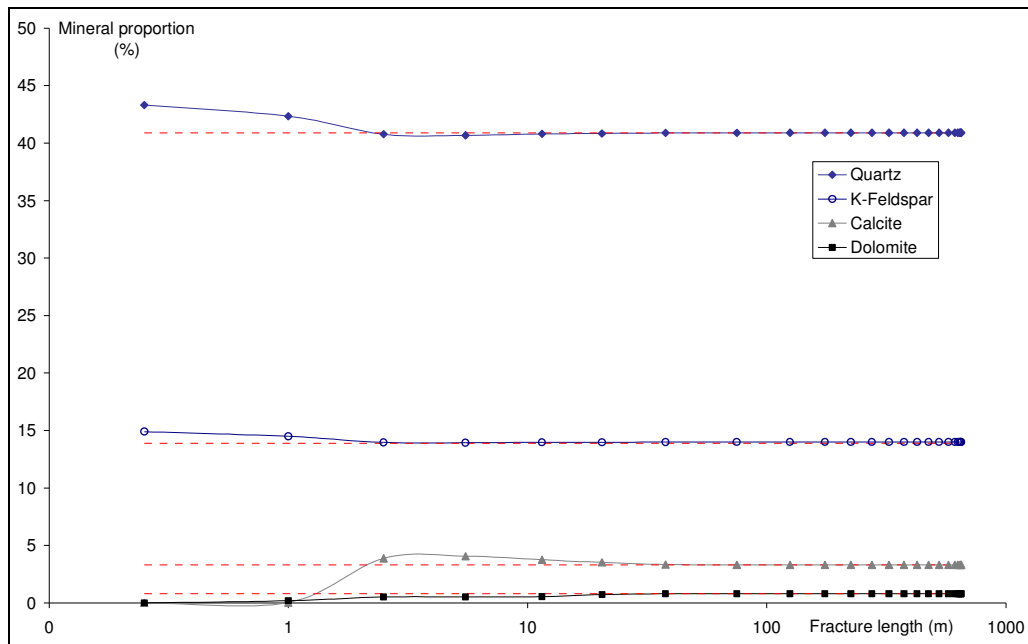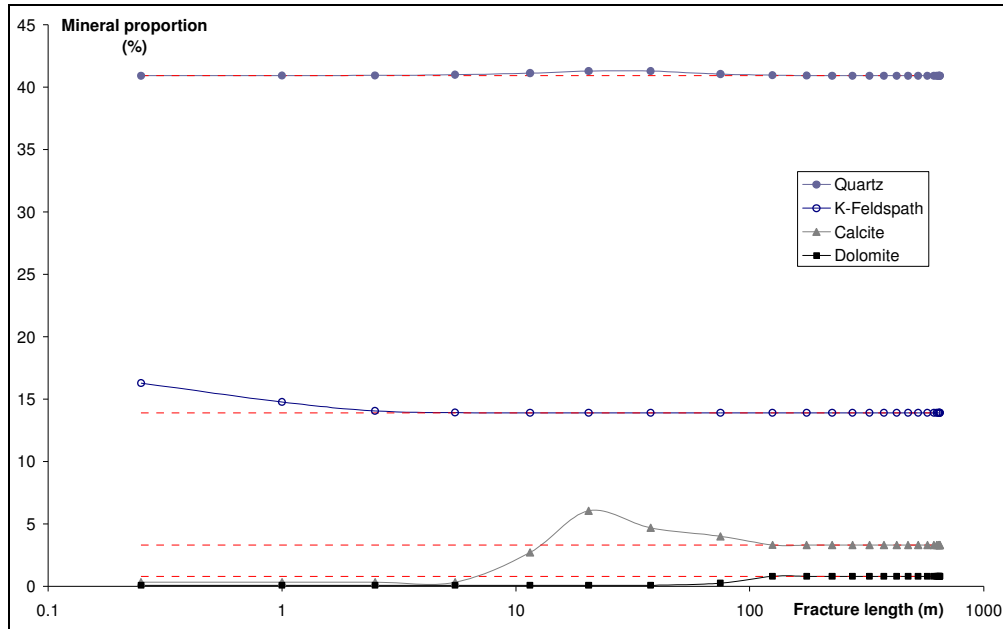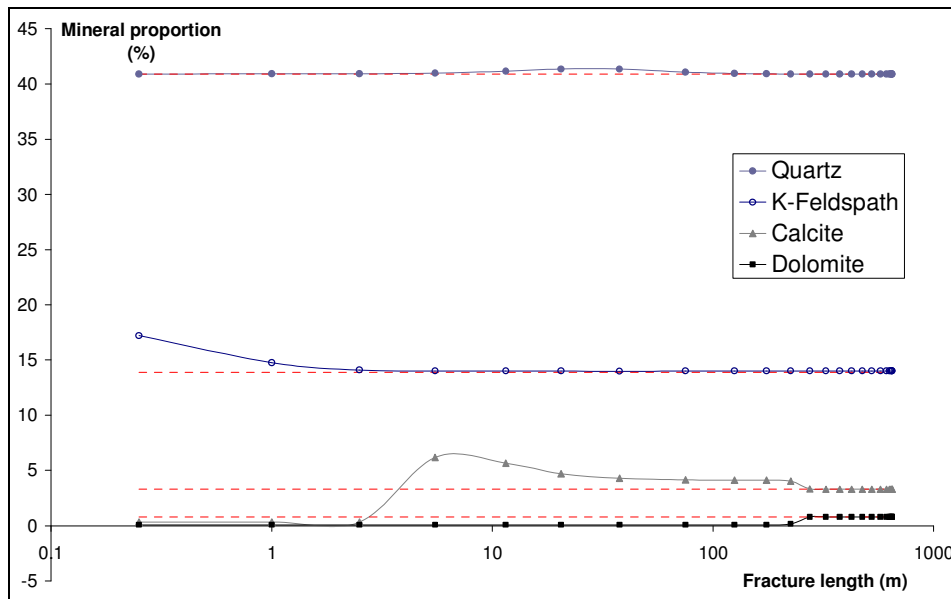

Figure 6-4. Evolution of the rock composition in the porous zone after 5 years of circulation simulated with Tr-Pitzer. The dashed lines correspond to initial concentrations.

6.5   IMPLICATIONS ON RESERVOIR PROPERTIES

The circulation of cooled fluid in the fracture zone affects the temperature of the reservoir within a distance of about 100 m from the injection well (Figure 6-5). Obviously, the temperature is lowest near the injection well (around 65°C), then increases to ambient reservoir temperatures (around 200°C) further away from the injection well. The predicted general trend of temperature with distance is similar for the three simulations. Temperature profiles take the shape of a front, which reaches mid-point temperatures (~132°C) somewhat closer to the injection well in the TOUGHREACT simulations compared to the FRACHEM simulation (Figure 6-5). The steeper front predicted with TOUGHREACT give rise to temperatures up to 30°C higher than FRACHEM-predicted temperatures at 20 to 50 m from the injection well. These differences diminish further away from the injection well and are attributed to the different model conceptualizations regarding heat transport.

Evolution of the reservoir porosity (Figure 6-6) is determined by the mineral reactions occurring in the reservoir. The three models give generally similar trends, although absolute changes in porosity vary significantly between models. With FRACHEM, the porosity is predicted to increase near the injection well because of the dissolution of calcite and dolomite. The porosity is enhanced by more than 50% at the injection well, but then decreases away from the well. Within a couple of meters from the injection well, the overall porosity change becomes negative because of calcite reprecipitation, resulting in a maximum overall porosity decrease close to 6%. At distances about 10 to 20 m away from the injection well, the porosity is predicted to remain essentially unaffected.

With Tr-DH, as with FRACHEM, the porosity is enhanced in the first 10 m from the injection well, due to the dissolution of carbonates. Calcite then precipitates between about 10 and 100 m, yielding a maximum porosity decrease of about 25% in this zone. However, the TOUGHREACT simulations show a trend of increasing porosity with distance along the fracture zone for the first several meters from the injection well (Figure 6-6). This increase results from feldspar precipitation near the injection well, impeding the porosity increase near the well. This precipitation is less prevalent in the FRACHEM simulations because the reservoir fluid is continuously recirculated in these simulations. In contrast, injection of the same initial fluid composition (Table 3-1, with pH 5.24) is simulated with TOUGHREACT. Simulations with Tr-Pitzer show a trend of porosity change with distance similar to that predicted with Tr-DH (Figure 6-6), except that calcite reprecipitation occurs closer to the injection well, which is more consistent with the FRACHEM results. This is expected, given that the solubility of calcite is overpredicted when activity coefficients are calculated using the Debye-Hückel model (Section 3). Again, calcite dissolution is the primary cause of porosity enhancement near the injection well.
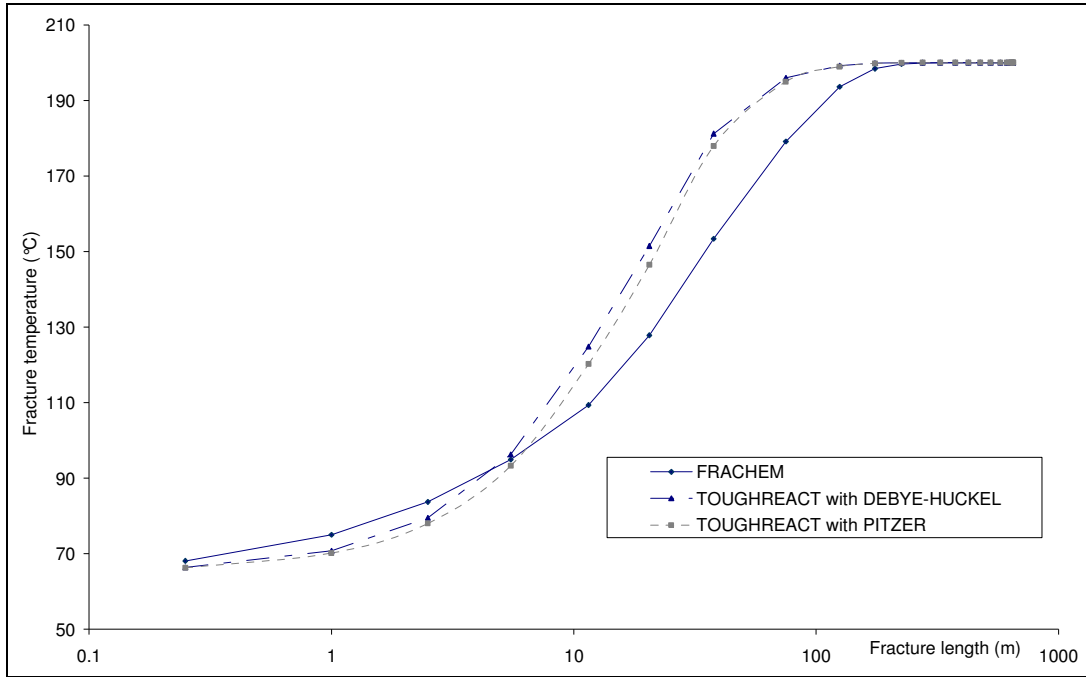
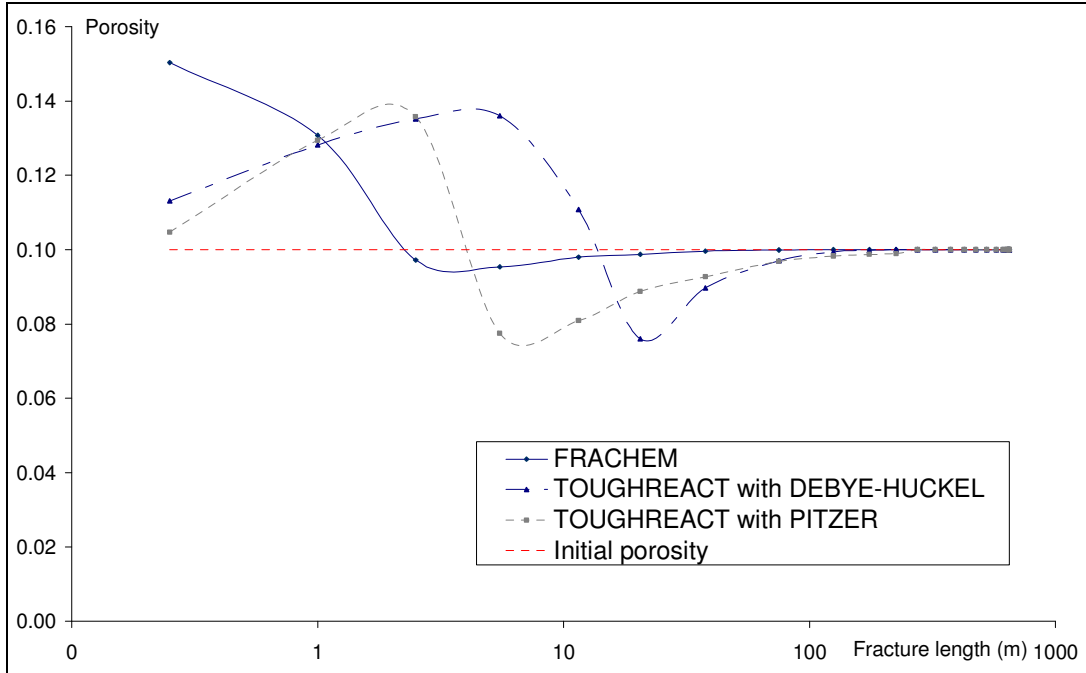Figure 6-5. Evolution of the reservoir temperature after 5 years of circulation.

Figure 6-6. Evolution of the reservoir porosity after 5 years of circulation.

7 CONCLUSIONS

The goals of this work were to compare two multicomponent reactive transport codes, FRACHEM (Durst, 2002; Bächler, 2003, Rabemanana et al. 2003; André et al., 2005; Bächler and Kohl, 2005) and TOUGHREACT (Xu and Pruess, 2001; Xu et al., 2004; Xu et al., 2006), to model complex water-rock interactions such as at the enhanced geothermal system at Soultz. In a first phase, different aspects of each code and input data were evaluated, including the methods to calculate activity coefficients, the mineral reaction rates, and the equilibrium constants of key minerals. The second phase of this study involved simulating the Soultz system.

TOUGHREACT offers the choice of either an extended Debye-Hückel (Tr-DH) model or the Pitzer formalism (Tr-Pitzer) to compute activity coefficients of dissolved species and water activity. FRACHEM uses activity coefficients externally calculated using TEQUIL (Moller et al., 1998). Activities of dissolved species computed with these codes for a typical Soultz fluid (ionic strength around 2 molal) were compared. Key differences were found in the activity coefficients of Ca^{2+} and Mg^{2+}, yielding calcite saturation indices lower by up to 1.5 $\log(Q/K)$ units when computed with Tr-DH instead of FRACHEM or Tr-Pitzer. However, the effect of increased calcite solubility in the Tr-DH simulations is minimal, because the model assumes an initial reservoir fluid composition reflecting saturation with respect to calcite. This shows that the model conceptualization is as important as the model input data. The Pitzer ion-interaction parameters implemented in TEQUIL are expected to provide more accurate calcite solubilities for applications with Soultz-type fluids, because these parameters were developed specifically for high-temperature geothermal applications at moderate ionic strengths. The relatively recent EQ3/6 Pitzer database *data0.ypf*, revised and used with TOUGHREACT in this study, is expected to be most accurate for applications below 150°C and very high ionic strengths.

Concerning the minerals reaction rates, a good agreement was observed for calcite, quartz and amorphous silica. For aluminosilicates (K-feldspar, albite and illite), differences in rates reach about two orders of magnitude, but can be explained easily by the fact that FRACHEM takes into consideration the inhibitor effect of Na^+, whereas TOUGHREACT does not. The largest differences in reaction rates were observed with dolomite and pyrite. In FRACHEM, kinetic data for these two minerals were determined from extrapolations that may be questionable. As a result some modifications to the future FRACHEM database should be considered.

The equilibrium constants for minerals used with FRACHEM and TOUGHREACT are mostly issued from the same sources. A good agreement is observed for the carbonates (calcite and dolomite) and for silicates (quartz and amorphous silica). The most important differences are observed for aluminosilicates, and these differences mainly result from the assumed form of aluminium in solution. Because reservoir pressures at Soultz are high (estimated to about 500 bar), pressure corrections to the equilibrium constants of carbonates and silica phases were investigated. For these minerals, the variation of equilibrium constants with pressure was implemented in FRACHEM using simple correlations. These correlations show that the equilibrium constants of carbonates increase significantly with pressure. For this reason, consideration should be given to implementing similar correlations into TOUGHREACT.

The codes were applied to simulate reactive transport processes in the Soultz reservoir, using essentially identical model conceptualizations and input chemical and hydrological data. Three

main processes were investigated for a fluid-injection period of 5 years: the evolution of reservoir temperature, the mineral precipitation/dissolution behavior, and the evolution of reservoir porosity. The three codes (FRACHEM, Tr-Pitzer, and Tr-DH) produced similar results. The circulation of cooled fluid in the fracture zone is predicted to affect the temperature of the reservoir within the first 100 m from the injection well. The injection of cooled fluid results in chemical disequilibrium and dissolution/precipitation reactions of several minerals. Carbonates dissolve at the injection well head (because of their retrograde solubility), whereas quartz and K-feldspar precipitate.   The dissolved calcite eventually reprecipitates away from the well, leading to an overall permeability decrease, which is predicted to range between 6% (with FRACHEM) and 25% (with Tr-DH and Tr-Pitzer). However, water-rock interactions occur mostly within the first 20 m from the injection well, and the porosity of the reservoir remains essentially unchanged at distances greater than about 100 m from the injection well. These results are consistent with a circulation test performed in 1997 within the shallow reservoir at 3,500 m at Soultz-sous-Forêts. The initial reservoir temperature was only 165°C, but the mineral composition of the granite was very similar to that in the deep reservoir (5000 m). During this circulation of 140 days, the pressure at the injection well decreased, indicating an increase of the injectivity around the injection well. According to the simulation presented in this report, this process is likely caused by the dissolution of carbonates, the most reactive minerals. It should also be noted that concentrations of dissolved silica in the injected fluid remain below the solubility of amorphous silica, even at a temperature of 65°C, and therefore porosity reduction from silica precipitation is avoided. This occurs because the reservoir temperature is relatively low (200°C), precluding the dissolution of silica at concentrations exceeding the 65°C solubility of amorphous silica (i.e., temperature remaining within a silica precipitation "gap"). Should injection occur in hotter intervals, amorphous silica precipitation in the injection well could be significant.

Although the three codes yield similar results, in a qualitative sense, quantitative results differ significantly (e.g., 6% versus 25% predicted porosity decrease at distances varying from about 2 to 20 m from the injection well, depending on the code).   These differences are primarily caused by differences in implemented activity coefficient models and their input parameters, as well as other model input thermodynamic and kinetic data. This study, therefore, highlights the importance of these data in reactive transport simulations, in particular for systems involving brines.

Reactive transport simulations are of enormous value in helping understanding processes at play, especially the various feedbacks between strongly coupled mechanisms.   However this study clearly shows that the predictive value of complex coupled THC simulations is mostly qualitative. Unless these simulations are closely integrated with field and laboratory experiments, their predictive ability should be asserted with much caution. Therefore, if THC simulations such as those presented here are to be used in a quantitative manner to plan the design and operation of the Soultz EGS (or any other geothermal system), integration of these simulations with laboratory experiments and field tests is highly recommended.

8   ACKNOWLEDGMENTS

INTENTIONALLY LEFT BLANK

9   REFERENCES

Alai, M., Sutton, M. and Carroll, S. (2005). Evaporative evolution of a Na-Cl-NO3-K-Ca-SO4-Mg-Si brine at 95 degrees C: Experiments and modeling relevant to Yucca Mountain, Nevada. *Geochem. Transactions*, 6(2), 31-45.

André, L., Rabemanana, V. and Vuataz, F.-D., (2005). Geochemical modelling of water-rock interactions and implications on the properties of the Soultz fractured reservoir. *Proceedings EHDRA Scientific Conference*, March 17-18, 2005, Soultz-sous-Forêts, France.

André, L., Spycher, N., Xu, T., Pruess, K. and Vuataz F.-D. (2006). Comparing FRACHEM and TOUGHREACT for reactive transport modelling of brine-rock interactions in enhanced geothermal systems (EGS). *Proceedings 31th Workshop on Geothermal Reservoir Engineering*, 30 Janvier – 1er Février, 2006, Stanford University, Stanford, California.

Arvidson, R.S. and Mackenzie, F.T., (1999). The dolomite problem: control of precipitation kinetics by temperature and saturation state. *Am. J. Sci.*, 299: 257-288.

Bächler, D., (2003), Coupled Thermal-Hydraulic-Chemical Modelling at the Soultz-sous-Forêts HDR reservoir (France). PhD thesis, ETH-Zürich, Switzerland, 150 p.

Bächler, D., Durst, P., Evans, K., Hopkirk, R., Kohl, Th., Megel, Th., Rabemanana, V. and Vuataz, F.-D., (2005). Studies and support for the Hot Fractured Rock reservoirs at Soultz-sous-Forêts. Final report for the Federal Office for Education and Science Project – OFES N° 00.0453.

Bauer, A. and Berger, G., (1998). Kaolinite and smectite dissolution rate in high molar KCl solutions at 35° and 80°C. *Appl. Geochem.*, 13: 905-916.

Bevan, J. and Savage, D., (1989). The effect of organic acids on the dissolution of K-feldspar under conditions relevant to burial diagenesis. *Mineralogical Magazine*, 53: 415-425.

Blum, A.E. and Stillings, L.L., (1995). Feldspar dissolution kinetics. In: A.F. White & S.L. Brantley (eds.), Chemical weathering rates of silicate minerals. *Mineralogical Society of America, Reviews in Mineralogy*, 31: 291-351.

Bolton, E.W., Lasaga, A.C. and Rye, D.M.,(1996). A model for the kinetic control of quartz dissolution and precipitation in porous media flow with spatially variable permeability; formulation and examples of thermal convection, *J. Geophys. Res., B, Solid Earth and Planets,* 101(10), 22157-22187.

Busenberg, E. and Plummer, L.N., (1982). The kinetics of dissolution of dolomite in CO_2-H_2O system at 1.5 to 65°C and 0 to 1 atm $P(CO_2)$. *Am. J. Sci.*, 282: 45-78.

Carroll, S., Mroczek, E., Alai, M. and Ebert, M., (1998). Amorphous silica precipitation (60 to 120°C): Comparison of laboratory and field rates. *Geochim. Cosmochim. Acta*, 62(8): 1379-1396.

Chou, L. and Wollast, R. (1985). Steady-state kinetics and dissolution mechanism of albite. *Am. J. Sci.*, 285: 963-993.

Dove, P. M. and Rimstidt, J. D., (1994). Silica-water interaction. In: P.J. Heaney, C.T. Prewitt & G.V. Gibbs (eds.), Silica: Physical behavior, geochemistry and materials applications. *Mineralogical Society of America, Reviews in Mineralogy*, 29: 259-308.

Durst, P., (2002). Geochemical modelling of the Soultz-sous-Forêts Hot Dry Rock test site: coupling fluid-rock interactions to heat and fluid transport. PhD Thesis, Neuchâtel, 127 pp.

Drummond, J. M., Jr. (1981). Boiling and mixing of hydrothermal fluids: Chemical effects on mineral precipitation, Ph.D. thesis, The Pennsylvania State University, University Park, Pennsylvania.

Ellis, A.J., (1963). The solubility of calcite in sodium chloride solutions at high temperature. *Am. J. Sci*., 261: 259-267.

Fournier, R.O. and Rowe, J., (1977). The solubility of amorphous silica in water at high temperatures and high pressures. *American Mineralogist*, 62: 1052-1056.

Fritz, B., (1981). Etude thermodynamique et modélisation des réactions hydrothermales et diagénétiques. *Sciences Géologiques*, *Mémoire*, 197 p.

Gautelier, M., Oelkers, E.H. and Schott, J., (1999). An experimental study of dolomite dissolution rates as a function of pH from -0.5 to 5 and temperature from 25 to 80ºC. *Chem. Geol.*, 157(1-2): 13-26.

Gautier, J.-M., Oelkers, E.H. and Schott, J., (1994). Experimental studies of K-feldspar dissolution rates as a fonction of chemical affinity at 150° and pH 9. *Geochim. Cosmochim. Acta*, 58(21): 4549-4560.

Genter, A., Traineau, H. and Artignan, D., (1997). Synthesis of geological and geophysical data at Soultz-sous-Forêts (France), *BRGM Report*, R 39440.

Gunnarsson, I. and Arnorsson, S., (2000). Amorphous silica solubility and the thermodynamic properties of H_4SiO_4 in the range of 0° to 350°C at P_{sat}. *Geochim. Cosmochim. Acta*, 64(13): 2295-2307.

Harvie, C.E., Moller, N. and Weare, J.H., (1984). The prediction of mineral solubilities in natural waters: The Na-K-Mg-Ca-H-Cl-SO_4-OH-HCO_3-CO_3-CO_2-H_2O system to high ionic strengths at 25°C. *Geochim. Cosmochim. Acta*, 48(4): 723-751.

He, S.L. and Morse, J.W. (1993). The carbonic-acid system and calcite solubility in aqueous Na-K-Ca-Mg-Cl-SO$_4$ solutions from 0 to 90-degrees-C. *Geochim. Cosmochim. Acta*, 57(15) 3533-3554

Helgeson, H.C. (1969). Thermodynamics of hydrothermal systems at elevated temperatures and pressures. *Am. J. Science*, 267, 729-804.

Helgeson, H.C., Delany, J.M., Nesbitt, H.W. and Bird, D.K., (1978). Summary and critique of the thermodynamic properties of rock-forming minerals. *Am. J. Sci.*, 278-A: 1-229.

Helgeson, H. C., Kirkham, D. H., Flowers, D. C. (1981). Theoretical prediction of the thermodynamic behavior of aqueous electrolytes at high pressures and temperatures: IV. Calculation of activity coefficients, osmotic coefficients, and apparent molal and standard and relative partial molal properties to 600 C and 5 kb. Am. J. Sci., v. 281, p. 1249–1516.

Helgeson, H.C., Murphy, W.M. and Aagaard, P., (1984). Thermodynamic and kinetic constraints on reaction rates among minerals and aqueous solutions. II. Rate constants, effective surface area, and the hydrolysis of feldspar. *Geochim. Cosmochim. Acta*, 48(12): 2405-2432.

Hellmann, R., (1994). The albite-water system: Part I. The kinetics of dissolution as a function of pH at 100, 200 and 300°C. *Geochim. Cosmochim. Acta*, 58(2): 595-611.

Huertas, F.J., Caballero, E., Jimenez de Cisneros, C., Huertas, F. and Linares, J., (2001). Kinetics of Montmorillonite dissolution in granitic solutions. *Appl. Geochem.*, 16: 397-407.

Icenhower, J.P. and Dove, P.M., (2000). The dissolution kinetics of amorphous silica into sodium chloride solutions: effects of temperature and ionic strength. *Geochim. Cosmochim. Acta*, 64(24): 4193-4203.

Jacquot, E., (2000). Modélisation thermodynamique et cinétique des réactions géochimiques entre fluides de bassin et socle cristallin: application au site expérimental du programme européen de recherche en géothermie profonde (Soultz-sous-Forêts, Bas-Rhin, France), PhD thesis, Université Louis Pasteur-Strasbourg I, France.

Johnson, J.W., Oelkers, E.H. and Helgeson, H.C., (1992). SUPCRT92: A software package for calculating the standard molal thermodynamic properties of minerals, gases, aqueous species, and reactions from 1 to 5000 bar and 0 to 1000°C. *Computers & Geosciences*, 18(7): 899-947.

Knauss, K.G. and Copenhaver, S.A., (1995). The effect of malonate on the dissolution kinetics of albite, quartz, and microcline as a fonction of pH at 70°C. *Appl. Geochem.*, 10: 17-33.

Kohl, T. and Hopkirk, R.J., (1995). "FRACTure" – A simulation code for forced fluid flow and transport in fractured, porous rock. *Geothermics*, 24(3), 333-343.

Kohl, T. and Rybach, L., (2001). Assessment of HDR reservoir geometry by inverse modelling of non-laminar hydraulic flow, *Proceedings, 26th Workshop on Geothermal Reservoir Engineering,* Stanford University, Stanford, California, January 29-31, 2001, 259-265.

Kohler, S.J., Dufaud, F. and Oelkers, E.H., (2003). An experimental study of illite dissolution kinetics as a function of pH from 1.4 to 12.4 and temperature from 5 to 50°C. *Geochim. Cosmochim. Acta*, 67(19): 3583-3594.

Langmuir, D. (1997). Aqueous Environmental Geochemistry, Prentice Hall, Upper Saddle River, New Jersey, 600pp.

Lasaga, A. C., (1984). Chemical kinetics of water-rock interactions. *J. Geophys. Res*., 89: 4009-4025.

Lasaga, A.C., Soler, J.M., Ganor, J., Burch, T.E. and Nagy, K.L., (1994). Chemical weathering rate laws and global geochemical cycles. *Geochim. Cosmochim. Acta*, 58: 2361-2386.

McKibben, M.A. and Barnes, H.L., (1986). Oxidation of pyrite in low temperature acidic solutions: Rate laws and surface textures. *Geochim. Cosmochim. Acta*, 50: 1509-1520.

Millero, F.J., (1982). The effect of pressure on the solubility of minerals in water and seawater. *Geochim. Cosmochim. Acta*, 46(1): 11-22.

Moller, N., Greenberg, J.P. and Weare, J.H., (1998). Computer modeling for geothermal systems: predicting carbonate and silica scale formation, CO_2 breakout and H_2S exchange. *Transp. porous media*, 33: 173-204.

Nagy, K.L., Blum, A.E. and Lasaga, A.C., (1991). Dissolution and precipitation kinetics of kaolinite at 80°C and pH 3: The dependence on solution saturation state. *Am. J. Sci.*, 291(7): 649-686.

Newton, R.C. and Manning, C.E., (2002). Experimental determination of calcite solubility in H_2O-NaCl solutions at deep crust/upper mantle pressures and temperature: Implications for metasomatic processes in shear zones. *American Mineralogist*, 87: 1401-1409.

Norton, D. and Knapp, R., (1977). Transport phenomena in hydrothermal systems; the nature of porosity, *Am. J. Sci.*, 277(8), 913-936.

Palandri, J.L. and Kharaka, Y.K., (2004). A compilation of rate parameters of water-mineral interaction kinetics for application of geochemical modelling. U.S. Geological Survey, Report 2004-1068.

Parkhurst, D.L. and Appelo, C.A.J. (1999). User's guide to PHREEQC (Version2) - A computer program for speciation, batch-reaction, one dimensional transport, and inverse

geochemical calculations. *U.S.Geological Survey Water-Resources Investigations,* Report 99-4259, 310 p.

Plummer, L.N., Wigley, T.M.L. and Parkhurst, D.L., (1978). The kinetics of calcite dissolution in CO_2-water systems at 5° to 60°C and 0.0 to 1.0 atm CO_2. *Am. J. Sci*., 278: 179-216.

Pruess, K., (1987). TOUGH user's guide, Nuclear Regulatory Commission, report NUREG/CR-4645 (also Lawrence Berkeley Laboratory Report LBL-20700, Berkeley, California), 1987.

Pruess, K., (1991). TOUGH2: A general numerical simulator for multiphase fluid and heat flow. Lawrence Berkeley Laboratory Report LBL-29400, Berkeley, California, 1991.

Pruess, K., Oldenburg, C. and Moridis, G., (1999). TOUGH2 user's guide, Version 2.0. Lawrence Berkeley Laboratory Report LBL-43134, Berkeley, California, 1999.

Rabemanana, V., Durst, P., Bächler, D., Vuataz, F.-D. and Kohl, Th., (2003). Geochemical modelling of the Soultz-sous-Forêts Hot Fractured Rock system: comparison of two reservoirs at 3.8 and 5 km depth. *Geothermics*, 32(4-6), 645-653.

Reed, M.H. (1982) Calculation of multicomponent chemical equilibria and reaction processes in systems involving minerals, gases and aqueous phase. *Geochim. Cosmochim. Acta*, 46: 513-528.

Reed, M.H. (1998). Calculation of simultaneous chemical equilibria in aqueous-mineral-gas systems and its application to modeling hydrothermal processes. In: *Techniques in Hydrothermal Ore Deposits Geology*, J. Richards and P. Larson (Eds), *Reviews in Economic Geology*, 10, 109-124.

Reed, M.H. and Spycher, N.F. (1998). User's guide for CHILLER: A program for computing water-rock reactions, boiling, mixing and other reaction processes in aqueous-mineral-gas systems and minplot guide, 3rd edition. Department of Geological Sciences, University of Oregon, Eugene, Or, USA.

Rickard, D., (1997). Kinetics of pyrite formation by the H_2S oxidation of iron (II) monosulfide in aqueous solutions between 25 and 125°C: The rate equation. *Geochim. Cosmochim. Acta*, 61(1): 115-134.

Rickard, D. and Luther, G. W., (1997). Kinetics of pyrite formation by the H_2S oxidation of iron (II) monosulfide in aqueous solutions between 25 and 125°C: The mechanism. *Geochim. Cosmochim. Acta*, 61(1): 135-147.

Rimstidt, J. D. and Barnes, H. L., (1980). The kinetics of silica-water reactions. *Geochim. Cosmochim. Acta*, 44(11): 1683-1699.

Rimstidt, J.D. (1997). Quartz solubility at low temperatures. *Geochim.Cosmochim. Acta*, 61(13): 2553-2558.

Rumpf, B. and Maurer, G. (1993). An experimental and theoretical investigation of the solubility of carbon-dioxide in aqueous solutions of strong electrolytes . Phys. Chem. Chem. Phys. 97(1): 85-97.

Rumpf, B. Nicolaisen, H, Ocal, C. and Maurer, G. (1994). Solubility of carbon-dioxyde in aqueous solutions of sodium chloride – Experimental results and correlation. *J Sol. Chem.*, 23(3): 431-448.

Shiraki, R. and Brantley, S. L., (1995). Kinetics of near-equilibrium calcite precipitation at 100°C: An evaluation of elementary reaction-based and affinity-based rate laws. *Geochim. Cosmochim. Acta*, 59(8): 1457-1471.

Sjoberg, E. L. and Rickard, D. T., (1984). Temperature dependence of calcite dissolution kinetics between 1 and 62°C at pH 2.7 to 8.4 in aqueous solutions. *Geochim. Cosmochim. Acta*, 48(3): 485-493.

Spencer, R.J., Moller, N. and Weare, J.H., (1990). The predictions of mineral solubilities in natural waters: A chemical equilibrium model for the Na-K-Ca-Mg-Cl-SO$_4$-H$_2$O system at temperatures below 25°C. *Geochim. Cosmochim. Acta*, 54: 575-590.

Steefel, C.I., and Lasaga, A.C., (1994). A coupled model for transport of multiple chemical species and kinetic precipitation/dissolution reactions with applications to reactive flow in single phase hydrothermal system. *Am. J. Sci.*, 294: 529-592.

Stillings, L.L. and Brantley, S.L., (1995). Feldspar dissolution at 25°C and pH 3: Reaction stoichiometry and the effect of cations. *Geochim. Cosmochim. Acta*, 59(8): 1483-1496.

Sverdrup, H., (1990). The kinetics of base cation release due to chemical weathering, Lund University Press, Lund, Sweden.

Talman, S.J., Wiwchar, B. and Gunter, W.D., (1990). Dissolution kinetics in the H$_2$O-CO$_2$ system along the steam saturation curve to 210°C. In Fluid-Mineral Interactions. Lancaster Press, Inc, San Antonio, Texas, pp. 41-55.

Tanger, J.C. and Helgeson, H.C., (1988). Calculations of the thermodynamic and transport properties of aqueous species at high pressures and temperatures: revised equations of state for the standard partial molal properties of ions and electrolytes. *Am. J. Sci.*, 288: 19-98.

Verma, A. and Pruess, K., (1988). Thermohydrological conditions and silica redistribution near high-level nuclear wastes emplaced in saturated geological formations. *J. Geophys. Res.*, 93: 1159-1173.

Vinsome, P. K. W. and Westerveld, J. (1980), A simple method for predicting cap and base rock heat losses in thermal reservoir simulators. *J. Canadian Pet. Tech.*, 19(3), 87–90.

Walther, J.V. and Helgeson, H.C., (1977). Calculation of the thermodynamic properties of aqueous silia and the solubility of quartz and its polymorphs at high pressures and temperatures. *Am. J. Sci.*, 277(10): 1315-1351.

White, S.P., (1995). Multiphase nonisothermal transport of systems of reacting chemicals. *Water Resour. Res.*, 31(7), 1761-1772.

Williamson, M. A. and Rimstidt, J. D., (1994). The kinetics and electrochemical rate-determining step of aqueous pyrite oxidation. *Geochim. Cosmochim. Acta*, 58(24): 5443-5454.

Wolery, T.J., (1992). A computer program for geochemical aqueous speciation solubility calculations: theoretical manual user's guide, and related documentation (Version 7.0). Lawrence Livermore Nat. Lab. Report, UCRL-MA-110662 PT III. 246 p.

Wolery, T.J. and Jarek, R.L. (2003). EQ3/6, Version 8.0, Software User's Manual, Software Document Number 10813-UM-8.0-00, *U.S. Department of Energy*, Office of Civilian Radioactive Waste Management, Office of Repository Development, 1261 Town Center Drive, Las Vegas, Nevada 89144, 2003.

Wolery, T.J., Jove-Colon, C., Rard, J. and Wijesinghe, A. (2004). Pitzer Database Development: Description of the Pitzer Geochemical Thermodynamic Database data0.ypf. Appendix I in *In-Drift Precipitates/Salts Model (P. Mariner)* Report ANL-EBS-MD-000045 REV 02. Las Vegas, Nevada: Bechtel SAIC Company.

Xu, T., Sonnenthal E., Spycher N., and Pruess, K., (2006). TOUGHREACT - A simulation program for non-isothermal multiphase reactive geochemical transport in variably saturated geologic Media: applications for geothermal injectivity and CO2 geologic sequestration. Computers and Geosciences, 32, 145-165.

Xu, T., Sonnenthal, E., Spycher, N. and Pruess, K. (2004). TOUGHREACT user's guide: a simulation program for non-isothermal multiphase reactive geochemical transport in variably saturated geologic media. Report LBNL-55460, Lawrence Berkeley National Laboratory, Berkeley, California.

Xu, T. and Pruess, K., (2001). Modeling multiphase fluid flow and reactive geochemical transport in variably saturated fractured rocks: 1. Methodology. *Am. J. Sci.*, 301: 16-33.

Xu, T., Sonnenthal, E., Spycher, N., Pruess, K., and Brimhall, G. (2001). Modeling multiphase fluid flow and reactive geochemical transport in variably saturated fractured rocks: 2. Applications to supergene copper enrichment and hydrothermal flows. *Am. J. Sci.*, 301: 34-59.

Xu, H., Sonnenthal, E.L., Spycher, N. and Pruess, K., (2004a). TOUGHREACT user's guide: a simulation program for nonisothermal multiphase reactive geochemical transport in variably saturated geologic media, Lawrence Berkeley National Laboratory, Berkeley, California, Report LBNL-55460, September 2004.

Xu, T., Ontoy, Y., Molling, P., Spycher, N., Parini, M. and Pruess, K., (2004b). Reactive transport modeling of injection well scaling and acidizing at Tiwi field, Philippines. Geothermics, 33(4): 477-491.

Zhang, G., Spycher, N., Xu, T., Sonnenthal, E., and Steefel, C., (2006a). Reactive geochemical transport modeling of concentrated aqueous solutions with TOUGHREACT — Supplement to TOUGHREACT users' guide for the Pitzer ion-interaction model. Report LBNL-57873, Lawrence Berkley National Laboratory, Berkeley, California (in review).

Zhang, G., Spycher, N., Sonnenthal, E., and Steefel, C. 2006, Implementation of a Pitzer activity model into TOUGHREACT for modeling concentrated solutions. Proceedings, *TOUGH Symposium 2006*, Lawrence Berkeley National Laboratory, Berkeley, California, May 15–17 (Report LBNL-60016).

Zhang, G., Zheng, Z. and Wan, J. (2004). Modeling reactive geochemical transport of concentrated aqueous solutions. *Water Resour. Res.*, 41(2), W02018.

Zysset, M. and Schindler, P.W., (1996). The proton promoted dissolution of K-montmorillonite. *Geochim. Cosmochim. Acta*, 60: 921-931.

APPENDIX 1: DISSOLUTION AND PRECIPITATION RATES

	Temperature	50	60	80	100	125	150	175	200
Calcite	-Log k_{diss}	4.873	4.767	4.572	4.397	4.201	4.027	3.870	3.729
	Log $k_{prec.}$ (Q/K<1.72)	-5.968	-5.752	-5.355	-5.000	-4.604	-4.253	-3.940	-3.659
	Log $k_{prec.}$ (Q/K>1.72)	-4.249	-4.033	-3.636	-3.280	-2.885	-2.534	-2.221	-1.939
Dolomite	-Log k_{diss}	6.278	6.221	6.115	6.019	5.911	5.814	5.727	5.648
	Log k_{prec}	-16.534	-15.886	-14.700	-13.642	-12.468	-11.433	-10.513	-9.691
Quartz	-Log k_{diss}	11.216	10.804	10.047	9.369	8.615	7.949	7.355	6.822
	Log k_{prec}	-12.314	-11.948	-11.282	-10.691	-10.042	-9.476	-8.978	-8.539
Amorphous silica	-Log k_{diss}	11.188	10.827	10.165	9.574	8.919	8.342	7.829	7.370
	Log k_{prec}	-9.352	-9.328	-9.284	-9.244	-9.200	-9.161	-9.127	-9.096
Pyrite	-Log k_{diss}	10.383	10.266	10.084	9.964	9.886	9.876	9.923	10.017
	Log k_{prec}	-14.550	-14.709	-14.949	-15.177	-15.561	-16.187	-17.268	-18.393
K-feldspar	-Log k_{diss}	13.726	13.475	13.016	12.606	12.152	11.751	11.395	11.076
	Log k_{prec}	-11.081	-10.751	-10.149	-9.611	-9.015	-8.489	-8.022	-7.605
Albite	-Log k_{diss}	15.601	15.354	14.901	14.496	14.044	13.645	13.288	12.966
	Log k_{prec}	-11.081	-10.751	-10.149	-9.611	-9.015	-8.489	-8.022	-7.605
Illite	-Log k_{diss}	14.026	13.822	13.436	13.082	12.685	12.332	12.017	11.734
	Log k_{prec}	-16.338	-15.757	-14.692	-13.741	-12.684	-11.751	-10.920	-10.176

Logarithm of dissolution and precipitation reaction rate (in $mol.m^2.s^{-1}$) as determined in FRACHEM code

	Temperature	50	60	80	100	125	150	175	200
Calcite	-Log k_{diss}	4.955	4.872	4.717	4.576	4.417	4.273	4.143	4.024
	Log k_{prec}	-5.491	-5.377	-5.168	-4.982	-4.776	-4.593	-4.432	-4.287
Sedimentary dolomite	-Log k_{diss}	5.186	5.009	4.683	4.392	4.066	3.777	3.517	3.283
	Log k_{prec}	-5.985	-5.732	-5.269	-4.855	-4.396	-3.991	-3.565	-3.310
Hydrothermal dolomite	-Log k_{diss}	5.478	5.200	4.686	4.216	3.673	3.161	2.573	2.196
	Log k_{prec}	-5.780	-5.318	-4.471	-3.716	-2.878	-2.140	-1.361	-0.896
Quartz	-Log k_{diss}	12.801	12.376	11.597	10.902	10.131	9.451	8.847	8.307
	Log k_{prec}	-12.801	-12.376	-11.597	-10.902	-10.131	-9.451	-8.847	-8.307
Amorphous silica	-Log k_{diss}	11.287	10.982	10.424	9.925	9.372	8.885	8.451	8.064
	Log k_{prec}	-10.000	-10.000	-10.000	-10.000	-10.000	-10.000	-10.000	-10.000
Pyrite	-Log k_{diss}	5.851	5.575	5.069	4.618	4.118	3.677	3.285	2.935
	Log k_{prec}	-9.627	-9.351	-8.845	-8.394	-7.894	-7.453	-7.061	-6.711
K-feldspar	-Log k_{diss}	11.576	11.355	10.946	10.573	10.153	9.777	9.437	9.130
	Log k_{prec}	-11.895	-11.711	-11.373	-11.072	-10.738	-10.443	-10.182	-9.948
Albite	-Log k_{diss}	11.166	10.835	10.228	9.685	9.082	8.550	8.076	7.652
	Log k_{prec}	-11.614	-11.275	-10.655	-10.102	-9.489	-8.947	-8.467	-8.037
Illite	-Log k_{diss}	12.022	11.874	11.595	11.336	11.035	10.754	10.490	10.239
	Log k_{prec}	-12.306	-12.136	-11.825	-11.548	-11.240	-10.969	-10.728	-10.512

Logarithm of dissolution and precipitation reaction rate (in $mol.m^2.s^{-1}$) as determined in TOUGHREACT code

INTENTIONALLY LEFT BLANK

APPENDIX 2: INPUT FILES

Chemical input files of FRACHEM: chem.dat

```
CHEM
 10.0  5000. .T.
 14 27  0
H2O        0.00 L 5.5515E+01     1.80000E+01  0.00000E+00
  0.938758E+00  0.531202E-03 -0.714763E-05  0.402949E-07 -0.771605E-10
Na+        1.00 L 1.1480E+00     23.0000E+00  0.00000E+00
  0.690774E+00  0.342080E-02 -0.368776E-04  0.114883E-06 -0.154321E-09
K+         1.00 L 7.3400E-02     39.0000E+00  0.00000E+00
  0.620091E+00  0.256082E-02 -0.264300E-04  0.768176E-07 -0.102881E-09
Ca++       2.00 L 0.1539E+00     40.0000E+00  0.00000E+00
  0.306380E+00 -0.198016E-03 -0.662294E-05  0.737311E-08  0.257202E-10
H+         1.00 L 1.2679E-05     1.00000E+00  0.00000E+00
  0.107989E+01  0.439006E-04 -0.205684E-04  0.811043E-07 -0.128601E-09
Cl-       -1.00 L 1.5269E+00     35.45000E+00  0.00000E+00
  0.601199E+00 -0.810744E-03 -0.102623E-05 -0.977366E-08  0.257202E-10
HCO3-     -1.00 L 9.4267E-04     61.0000E+00  0.00000E+00
  0.360300E+00  0.389609E-03 -0.135957E-04  0.442387E-07 -0.514403E-10
SO4--     -2.00 L 6.5974E-04     96.0000E+00  0.00000E+00
  0.522115E-01 -0.150909E-03 -0.197436E-05  0.997771E-08 -0.110597E-10
H4SiO4     0.00 L 6.0600E-03     96.0000E+00  0.00000E+00
  0.143047E+01 -0.594297E-02  0.599280E-04 -0.291495E-06  0.514403E-09
FE++       2.00 L 2.4000E-03     55.8500E+00  0.00000E+00
  0.126180E+00 -0.210151E-02  0.162531E-04  0.000000E+00  0.000000E+00
MG++       2.00 L 4.6050E-03     24.3000E+00  0.00000E+00
  0.314857E+00 -0.283000E-02  0.942857E-05  0.000000E+00  0.000000E+00
HS-       -1.00 L 9.8500E-04     33.0000E+00  0.00000E+00
  0.210969E-03 -0.507186E-05  0.877067E-07 -0.609429E-09  0.136579E-11
Al+++      3.00 L 3.7000E-06     26.9815E+00  0.00000E+00
  0.102442E-01 -0.213274E-03  0.169612E-05 -0.609318E-08  0.832131E-11
CO3--     -2.00 L 3.0182E-07     60.0000E+00  0.00000E+00
  0.382177E-01 -0.245813E-03 -0.143158E-06  0.378258E-08 -0.668724E-11
OH-       -1.00 L 2.8449E-06     17.0000E+00  0.00000E+00
  0.406520E+00  0.860523E-04 -0.101955E-04  0.212620E-07 -0.174868E-21
Ca(HCO3)+  1.00 L 1.1105E-18     101.000E+00  0.00000E+00
  0.486211E+00  0.539741E-03 -0.109594E-04  0.269204E-07 -0.257202E-10
CO2(aq)    0.00 L 1.6524E-02     44.0000E+00  0.00000E+00
  0.139083E+01 -0.142460E-02  0.171039E-04 -0.111454E-06  0.257202E-09
CaCO3(aq)  0.00 L 7.0223E-07     100.000E+00  0.00000E+00
  0.100000E+01  0.000000E+00  0.000000E+00  0.000000E+00  0.000000E+00
CASO4(AQ)  0.00 L 2.7056E-04     136.000E+00  0.00000E+00
  0.100000E+01  0.000000E+00  0.000000E+00  0.000000E+00  0.000000E+00
QUARTZ     0.00 S 8.18E+00       60.0000E+00  2.65000E+03
  0.100000E+01  0.000000E+00  0.000000E+00  0.000000E+00  0.000000E+00
CALCITE    0.00 S 8.30E00        100.000E+00  2.71000E+03
  0.100000E+01  0.000000E+00  0.000000E+00  0.000000E+00  0.000000E+00
DOLOMITE   0.00 S 1.15E+00       184.300E+00  2.71000E+03
  0.100000E+01  0.000000E+00  0.000000E+00  0.000000E+00  0.000000E+00
PYRITE     0.00 S 2.72E+00       119.850E+00  5.00000E+03
  0.100000E+01  0.000000E+00  0.000000E+00  0.000000E+00  0.000000E+00
SILICAM    0.00 S 159.2E+00      60.0000E+00  2.07000E+03
  0.100000E+01  0.000000E+00  0.000000E+00  0.000000E+00  0.000000E+00
KFELDS     0.00 S 11.54E+00      278.330E+00  2.50000E+03
  0.100000E+01  0.000000E+00  0.000000E+00  0.000000E+00  0.000000E+00
ALBITE     0.00 S 13.45E+00      262.220E+00  2.61000E+03
  0.100000E+01  0.000000E+00  0.000000E+00  0.000000E+00  0.000000E+00
ILLITE     0.00 S 13.12E+00      389.340E+00  2.75000E+03
```

```
 0.100000E+01  0.000000E+00  0.000000E+00  0.000000E+00  0.000000E+00
CO3--
  0.00   0.00   0.00   0.00  -1.00   0.00   1.00   0.00   0.00   0.00   0.00   0.00   0.00 1
 0.106210E+02 -0.141799E-01  0.119948E-03 -0.377598E-06  0.563170E-09
OH-
  1.00   0.00   0.00   0.00  -1.00   0.00   0.00   0.00   0.00   0.00   0.00   0.00   0.00 1
 0.149397E+02 -0.427928E-01  0.221928E-03 -0.752711E-06  0.129450E-08
Ca(HCO3)+
  0.00   0.00   0.00   1.00   0.00   0.00   1.00   0.00   0.00   0.00   0.00   0.00   0.00 1
-0.009172E+01  0.377718E-02 -0.100084E-03  0.355916E-06 -0.566154E-09
CO2(aq)
 -1.00   0.00   0.00   0.00   1.00   0.00   1.00   0.00   0.00   0.00   0.00   0.00   0.00 1
-0.657655E+01  0.122524E-01 -0.143343E-03  0.466424E-06 -0.666853E-09
CaCO3(aq)
  0.00   0.00   0.00   1.00  -1.00   0.00   1.00   0.00   0.00   0.00   0.00   0.00   0.00 1
 0.750075E+01 -0.218770E-01  0.865748E-04 -0.237638E-06  0.206620E-09
CASO4(AQ)
  0.00   0.00   0.00   1.00   0.00   0.00   0.00   1.00   0.00   0.00   0.00   0.00   0.00 1
-0.207040E+01 -0.255960E-03 -0.654052E-04  0.314719E-06 -0.770838E-09
QUARTZ
 -2.00   0.00   0.00   0.00   0.00   0.00   0.00   0.00   1.00   0.00   0.00   0.00   0.00 5
-0.450127E+01  0.230740E-01 -0.136254E-03  0.554763E-06 -0.955384E-09
0 .1 .1 1 0
CALCITE
  0.00   0.00   0.00   1.00  -1.00   0.00   1.00   0.00   0.00   0.00   0.00   0.00   0.00 5
 0.222690E+01 -0.154277E-01  0.866480E-05  0.164848E-07 -0.126807E-09
0 .1 .1 2 0
DOLOMITE
  0.00   0.00   0.00   1.00  -2.00   0.00   2.00   0.00   0.00   0.00   1.00   0.00   0.00 5
 0.340778E+01 -0.370318E-01  0.430942E-04 -0.191080E-07 -0.215571E-09
0 .1 .1 3 0
PYRITE
 -1.00   0.00   0.00   0.00   0.25   0.00   0.00   0.25   0.00   1.00   0.00   1.75   0.00 5
-0.265025E+02  0.836345E-01 -0.427566E-03  0.142557E-05 -0.247958E-08
0 .1 .1 4 0
SILICAM
 -2.00   0.00   0.00   0.00   0.00   0.00   0.00   0.00   1.00   0.00   0.00   0.00   0.00 5
-0.296646E+01  0.976023E-02 -0.251011E-04  0.273648E-07 -0.822790E-11
0 .1 .1 5 0
KFELDS
 -4.00   0.00   1.00   0.00  -4.00   0.00   0.00   0.00   3.00   0.00   0.00   0.00   1.00 5
 0.454871E+00 -0.144933E-01 -0.509821E-04  0.507837E-06 -0.109326E-08
0 .1 .1 6 0
ALBITE
 -4.00   1.00   0.00   0.00  -4.00   0.00   0.00   0.00   3.00   0.00   0.00   0.00   1.00 5
 0.541616E+01 -0.415801E-01 +0.381644E-04  0.331536E-06 -0.931468E-09
0 .1 .1 7 0
ILLITE
 -2.00   0.00   0.60   0.00  -8.00   0.00   0.00   0.00   3.50   0.00   0.25   0.00   2.30 5
 0.134375E+02 -0.133928E+00  0.461581E-03 -0.999223E-06  0.100997E-08
0 .1 .1 8 0
INJ
1
3 -1
PROD
1
15 -1
SURF
2000.0  65.0d0  0.0e6
ENDFI
```

Chemical input files of TOUGHREACT and DEBYE-HUCKEL: chemical.inp

'Soultz - Febr-18-05
'--'
'DEFINITION OF THE GEOCHEMICAL SYSTEM'
'PRIMARY AQUEOUS SPECIES'
'h2o'
'h+'
'ca+2'
'mg+2'
'na+'
'k+'
'cl-'
'sio2(aq)'
'hco3-'
'so4-2'
'alo2-'
'*'
'AQUEOUS COMPLEXES'
'al+3'
'caco3(aq)'
'cahco3+'
'caso4(aq)'
'co3-2'
'co2(aq)'
'oh-'
'*'
'MINERALS'
'quartz'   1   3   0   0
          1.2589e-14 0 1.0 1.0 87.5 0.0 0.0 0.0   ! prec.
          1.2589e-14 0 1.0 1.0 87.5 0.0 0.0 0.0 1.e-6   0   1.0000e+02 0 1.0 1.0 00.0 1.174 -0.002028 -4158.0 1.e-6
0
0.0   0.0   000.00
'k-feldspar'   1   3   0   0
          3.8905e-13   2   1.0 1.0 38.00 0.0 0.0 0.0
                2
                8.7096e-11   51.7   1   'h+'   0.5   ! acid mechanism
                6.3096e-22   94.1   1   'h+' -0.823   ! base
          3.8905e-13 0 1.0 1.0 38.00 0.0 0.0 0.0 1.e-6   0
0.0   0.   000.00
'calcite'   1   3   0   0
          1.5488e-06   2   1.0 1.0 23.50 0.0 0.0 0.0
                1
                5.0119e-01 14.40   1   'h+'   1.0
          1.5488e-6   0   1.0 1.0 23.50 0.0 0.0 0.0 1.e-6   0
0.0   0.   000.00
'dolomite'   1   3   0   0
          2.9512e-08   2   1.0 1.0 52.20 0.0 0.0 0.0
                1
                6.4565e-04 36.1   1   'h+'   0.5
          2.9512e-08   0   1.0 1.0 52.20 0.0 0.0 0.0 1.e-6   0
0.0   0.   000.00
'*' 0 0 0   0
'GASES'
'*'
'SURFACE COMPLEXES'
'*'
'species with Kd and decay   decay constant(1/s)'
'*'   0.0d0
'EXCHANGEABLE CATIONS'
'   master   convention   ex. coef.'
'*'   0   0   0.0

```
'------------------------------------------------------------------------'
'INITIAL AND BOUNDARY WATER TYPES'
2  0  0   !niwtype, nbwtype, nrwtype= number of ini, bound, rech waters
1   200.0   0                !iwtype initial, temp (C)
'   icon      guess      ctot       constrain'      ! Vein alteration
h2o      1   0.1000E+01   0.10000E+01
h+       1   0.1000E-04   0.15617E+00
ca+2     1   0.1000E-00   0.16950E+00
mg+2     1   0.5000E-02   0.32100E-02
na+      1   0.1150E+01   0.11480E+01
k+       1   0.7000E-01   0.73400E-01
fe+2     1   0.2000E-02   0.26140E-02
cl-      1   0.1500E+01   0.16480E+01
sio2(aq) 1   0.6000E-02   0.60600E-02
hco3-    1   0.9000E-03   0.16002E+00
so4-2    1   0.6500E-03   0.17714E-02
alo2-    1   0.3700E-05   0.37000E-04
'*'      0      0.0         0.0         ' '    0
2   65.0   0                  !iwtype initial, temp (C)
'   icon      guess      ctot       constrain'      ! Vein alteration
h2o      1   0.1000E+01   0.10000E+01
h+       1   0.1000E-04   0.15617E+00
ca+2     1   0.1000E-00   0.16950E+00
mg+2     1   0.5000E-02   0.32100E-02
na+      1   0.1150E+01   0.11480E+01
k+       1   0.7000E-01   0.73400E-01
fe+2     1   0.2000E-02   0.26140E-02
cl-      1   0.1500E+01   0.16480E+01
sio2(aq) 1   0.6000E-02   0.60600E-02
hco3-    1   0.9000E-03   0.16002E+00
so4-2    1   0.6500E-03   0.17714E-02
alo2-    1   0.3700E-05   0.37000E-04
'*'      0      0.0         0.0         ' '    0
'------------------------------------------------------------------------'
'INITIAL MINERAL ZONES'
 1
 1
'mineral       vol.frac. '              ! Vein alteration
'quartz'       0.409      1
1.0e-5         98.0e-1        0
'k-feldspar'   0.139      1
1.0e-5         98.0e-1        0
'calcite'      0.033      1
1.0e-5         98.0e-1        0
'dolomite'     0.008      1
1.0e-5         98.0e-1        0
'*'            0.0        0
'------------------------------------------------------------------------'
'INITIAL gas ZONES'
1                        !ngtype= number of gas zones
1                        !igtype
'gas     partial pressure'   !at 25 C equil w/ water
'*'          0.0
'------------------------------------------------------------------------'
'Permeability-Porosity Zones'
 1
 1
'perm law   a-par   b-par tcwM1'       ! Fractured vein
   5     0.16    2.0           ! PHIc=0.16, n(power term)=2
'------------------------------------------------------------------------'
'INITIAL SURFACE ADSORPTION ZONES'
0                        !ndtype= number of sorption zones
```

```
'zone      ad.surf.(m2/kg)  total ad.sites (mol/l)'
'--------------------------------------if Sden=0 Kd store retardation factor'
'INITIAL LINEAR EQUILIBRIUM Kd ZONE'
1                                        !kdtpye=number of Kd zones
1                                        !idtype
'species   solid-density(Sden,kg/dm**3)  Kd(l/kg=mass/kg solid / mass/l'
'*'        0.0           0.0
'--------------------------------------if Sden=0 Kd store retardation factor'
'INITIAL ZONES OF CATION EXCHANGE'
0                      !nxtype= number of exchange zones
'zone         ex. capacity'
'----------------------------------------------------------------------'

'end'
```

Chemical input files of TOUGHREACT and PITZER: extract from chemical.inp

The only difference with the file presented above concerns the water composition

```
/……
'----------------------------------------------------------------------'
'INITIAL AND BOUNDARY WATER TYPES'
2  0  0  !niwtype, nbwtype, nrwtype= number of ini, bound, rech waters
1    200.0   0                !iwtype initial, temp (C)
'    icon      guess       ctot      constrain'     ! Vein alteration
h2o      1   0.1000E+01   0.10000E+01
h+       1   0.1000E-04   0.32305E-02
ca+2     1   0.1000E-00   0.16950E+00
mg+2     1   0.5000E-02   0.32100E-02
na+      1   0.1150E+01   0.11480E+01
k+       1   0.7000E-01   0.73400E-01
fe+2     1   0.2000E-02   0.26140E-02
cl-      1   0.1500E+01   0.16480E+01
sio2(aq) 1   0.6000E-02   0.60600E-02
hco3-    1   0.9000E-03   0.74998E-02
so4-2    1   0.6500E-03   0.17710E-02
alo2-    1   0.3700E-05   0.37000E-04
'*'    0       0.0        0.0       ' '   0
2    65.0   0                     !iwtype initial, temp (C)
'    icon      guess       ctot      constrain'     ! Vein alteration
h2o      1   0.1000E+01   0.1000E+01
h+       1   0.1000E-04   0.32305E-02
ca+2     1   0.1000E-00   0.16950E+00
mg+2     1   0.5000E-02   0.32100E-02
na+      1   0.1150E+01   0.11480E+01
k+       1   0.7000E-01   0.73400E-01
fe+2     1   0.2000E-02   0.26140E-02
cl-      1   0.1500E+01   0.16480E+01
sio2(aq) 1   0.6000E-02   0.60600E-02
hco3-    1   0.9000E-03   0.74998E-02
so4-2    1   0.6500E-03   0.17710E-02
alo2-    1   0.3700E-05   0.37000E-04
'*'    0       0.0        0.0       ' '   0
/ ………
```

Flow input files of TOUGHREACT: flow.inp

```
# Batch model for initializing water chemistry, Soultz site
ROCKS----1----*----2----*----3----*----4----*----5----*----6----*----7----*----8
VEINA   1    2650.      0.10  0.55E-12  0.55E-12  0.55E-12      2.9        0.
                              0.3
CONBD   1    2650.      0.02  1.0E-18   1.0E-18   1.0E-18       3.0      1000.
                              0.05


START
REACT----1MOPR(20)-2----*----3----*----4----*----5----*----6----*----7----*----8
00020000231000                              ! 5(1, HMW)1(0)0
PARAM----1 MOP: 123456789*123456789*1234 ---*----5----*----6----*----7----*----8
   29999    90000000001000200014000005000
           1.5768E08      -1.0  8.64E02                 9.81
     1.E00     1.E00     1.E00     1.E00     1.E00     1.E00     1.E00     1.E00
     1.E-7        1.       0.1        1.        1.      1.E-8
 0.5000000000000E+08 0.2000000000000E+03
RPCAP----1----*----2----*----3----*----4----*----5----*----6----*----7----*----8
    1        0.33333      0.05        1.        1.
    1            0.        1.
TIMES----1----*----2----*----3----*----4----*----5----*----6----*----7----*----8
    9
   8.64E048.6400E+052.5920E+061.55520E07 3.1104E07 6.3072E07 9.4608E071.26144E08
 1.5768E08
ELEME----1----*----2----*----3----*----4----*----5----*----6----*----7----*----8
    1              10.2500E+000.1000E+02           0.2500E+000.5000E+01-.2500E-01
    2              10.5000E+000.2000E+02           0.1000E+010.5000E+01-.2500E-01
    3              10.1000E+010.4000E+02           0.2500E+010.5000E+01-.2500E-01
    4              10.2000E+010.8000E+02           0.5500E+010.5000E+01-.2500E-01
    5              10.4000E+010.1600E+03           0.1150E+020.5000E+01-.2500E-01
    6              10.5000E+010.2000E+03           0.2050E+020.5000E+01-.2500E-01
    7              10.1225E+020.4900E+03           0.3775E+020.5000E+01-.2500E-01
    8              10.2500E+020.1000E+04           0.7500E+020.5000E+01-.2500E-01
    9              10.2500E+020.1000E+04           0.1250E+030.5000E+01-.2500E-01
   10              10.2500E+020.1000E+04           0.1750E+030.5000E+01-.2500E-01
   11              10.2500E+020.1000E+04           0.2250E+030.5000E+01-.2500E-01
   12              10.2500E+020.1000E+04           0.2750E+030.5000E+01-.2500E-01
   13              10.2500E+020.1000E+04           0.3250E+030.5000E+01-.2500E-01
   14              10.2500E+020.1000E+04           0.3750E+030.5000E+01-.2500E-01
   15              10.2500E+020.1000E+04           0.4250E+030.5000E+01-.2500E-01
   16              10.2500E+020.1000E+04           0.4750E+030.5000E+01-.2500E-01
   17              10.2500E+020.1000E+04           0.5250E+030.5000E+01-.2500E-01
   18              10.2500E+020.1000E+04           0.5750E+030.5000E+01-.2500E-01
   19              10.1225E+020.4900E+03           0.6122E+030.5000E+01-.2500E-01
   20              10.5000E+010.2000E+03           0.6295E+030.5000E+01-.2500E-01
   21              10.4000E+010.1600E+03           0.6385E+030.5000E+01-.2500E-01
   22              10.2000E+010.8000E+02           0.6445E+030.5000E+01-.2500E-01
   23              10.1000E+010.4000E+02           0.6475E+030.5000E+01-.2500E-01
   24              10.5000E+000.2000E+02           0.6490E+030.5000E+01-.2500E-01
   25              10.2500E+000.1000E+02           0.6498E+030.5000E+01-.2500E-01
L   1              10.2000E+310.0000E+00           0.0000E+000.0000E+000.0000E+00
   30              10.2000E+310.0000E+00           0.6510E+030.0000E+000.0000E+00
con00          CONBD

CONNE----1----*----2----*----3----*----4----*----5----*----6----*----7----*----8
    1   2                  10.2500E+000.5000E+000.5000E+00
    2   3                  10.5000E+000.1000E+010.5000E+00
    3   4                  10.1000E+010.2000E+010.5000E+00
    4   5                  10.2000E+010.4000E+010.5000E+00
    5   6                  10.4000E+010.5000E+010.5000E+00
    6   7                  10.5000E+010.1225E+020.5000E+00
```

```
     7     8                      10.1225E+020.2500E+020.5000E+00
     8     9                      10.2500E+020.2500E+020.5000E+00
     9    10                      10.2500E+020.2500E+020.5000E+00
    10    11                      10.2500E+020.2500E+020.5000E+00
    11    12                      10.2500E+020.2500E+020.5000E+00
    12    13                      10.2500E+020.2500E+020.5000E+00
    13    14                      10.2500E+020.2500E+020.5000E+00
    14    15                      10.2500E+020.2500E+020.5000E+00
    15    16                      10.2500E+020.2500E+020.5000E+00
    16    17                      10.2500E+020.2500E+020.5000E+00
    17    18                      10.2500E+020.2500E+020.5000E+00
    18    19                      10.2500E+020.1225E+020.5000E+00
    19    20                      10.1225E+020.5000E+010.5000E+00
    20    21                      10.5000E+010.4000E+010.5000E+00
    21    22                      10.4000E+010.2000E+010.5000E+00
    22    23                      10.2000E+010.1000E+010.5000E+00
    23    24                      10.1000E+010.5000E+000.5000E+00
    24    25                      10.5000E+000.2500E+000.5000E+00
 L   1     1                      10.1000E-030.5000E-010.1000E+010.0000E+00
    25    30                      10.1000E+020.1000E+010.1000E+010.0000E+00


INCON----1----*----2----*----3----*----4----*----5----*----6----*----7----*----8
 L   1                           0.1
             0.58E+08                 0.65E+02


ENDCY

MESHMAKER1----*----2----*----3----*----4----*----5----*----6----*----7----*----8
XYZ

NX      25          0.
5.0000e-011.0000e-002.0000e-004.0000E-008.0000E-001.0000E+012.4500E+015.0000E+01
5.0000E+015.0000E+015.0000E+015.0000E+015.0000E+015.0000E+015.0000E+015.0000E+01
5.0000E+015.0000E+012.4500E+011.0000E+018.0000E+004.0000E+002.0000E+001.0000E+00
5.0000E-01
NY      11.0000E+01
NZ      15.0000E-02


ENDFI----1----*----2----*----3----*----4----*----5----*----6----*----7----*----8
```